

AN INTEGRATED CONCEPTUAL DESIGN WORKFLOW FOR LIQUID HYDROGEN-POWERED BOX-WING AIRCRAFT

Giuseppe Palaia[1], Karim Abu Salem[2], Alessandro A. Quarta[3] & Pedro D. Bravo-Mosquera[4]

[1]Department of Mechanical and Aerospace Engineering, Politecnico di Torino, Torino, Italy
[2]Department of Civil, Environmental and Mechanical Engineering, Università degli Studi di Trento, Trento, Italy
[3]Department of Civil and Industrial Engineering, University of Pisa, Pisa, Italy
[4]São Carlos School of Engineering, University of São Paulo (EESC / USP), São Carlos, SP, Brazil

Abstract

The present work presents an integrated conceptual design workflow for liquid-hydrogen-powered box-wing aircraft. The study addresses a limitation of many early hydrogen-aircraft investigations, in which the airframe is largely inherited from a conventional kerosene configuration and cryogenic storage is introduced as a retrofit constraint. In contrast, the proposed workflow treats the hydrogen storage system as a design driver that affects geometry, usable fuselage volume, payload accommodation, tank dry mass, fuel inventory, boil-off, venting, mission performance and maximum take-off weight consistency. The computational chain is implemented in a parametric simulation environment and links aircraft geometry generation, aerodynamic database construction, conceptual mass estimation, liquid-hydrogen tank design, coupled mission and two-phase tank thermodynamic simulation, reserve assessment and fixed-point take-off mass convergence. The box-wing architecture is used as the reference application because its joined lifting system and fuselage-volume allocation provide a relevant test case for hydrogen integration under airport-span constraints. Numerical demonstrations are presented for a medium-range box-wing family, redesign-aware wing-area variations, insulation and venting sensitivities, cross-class applications and preliminary design-of-experiments data. The results show that increasing cylindrical tank length simultaneously modifies passenger capacity, dry tank mass, liquid-hydrogen mass, venting losses and nominal range; therefore storage volume cannot be assessed independently of cabin layout and aircraft-level mass consistency. They also show that retaining the lifting-surface area of an inherited configuration may lead to non-optimal cruise operation after hydrogen integration changes the mass state. The proposed workflow does not deliver a final optimized aircraft, but establishes a transparent and auditable conceptual framework for exploring hydrogen-powered box-wing aircraft families and for generating structured datasets suitable for future surrogate modelling and multidisciplinary optimization.

Keywords: box-wing architecture; liquid hydrogen; conceptual aircraft design; mission simulation; green aviation

1. Introduction

Commercial aviation is under increasing pressure to reduce its environmental impact while preserving the connectivity, reliability and productivity that make air transport a strategic component of modern mobility. The reduction of climate impact cannot be addressed by a single technological change: it requires progress in propulsion, energy carriers, aircraft efficiency, operations, infrastructure and design methods [1–3]. Within this broad transition, hydrogen has received renewed attention because it can remove direct carbon dioxide emissions during aircraft operation and because its specific energy is significantly higher than that of conventional kerosene. Recent reviews have therefore discussed hydrogen-powered aircraft as a relevant research direction for future civil aviation, while also emphasizing that its overall environmental value depends on production pathways, infrastructure, propulsion technology and non-carbon climate effects [4–9].

Hydrogen, however, is not a drop-in replacement for current aviation fuel. Its advantages and limitations are both rooted in its physical properties. On the one hand, hydrogen offers high gravimetric energy content and can be used either in combustion-based propulsion systems or, for some aircraft classes, through more advanced fuel-cell-based architectures. On the other hand, its volumetric energy density is low, and gaseous storage at ambient conditions is incompatible with the volume constraints of transport aircraft. For medium-range and larger applications, liquid hydrogen is generally considered a more realistic storage state, because liquefaction increases density and reduces the tank volume required onboard. This choice introduces cryogenic temperatures, dedicated insulation, pressure management, boil-off, venting, safety constraints and airport-infrastructure implications [10–14]. As a consequence, hydrogen should not be regarded only as a different source of energy. At aircraft level, it modifies the relationship between energy storage, internal volume, mass distribution, payload capability and mission performance, including the specific integration of advanced cryogenic tanks and the management of their thermal state.

These couplings are particularly important during conceptual design. In conventional kerosene aircraft, fuel is usually stored in the wing, with limited direct interference with passenger accommodation and cargo volume. Liquid hydrogen tanks are instead typically installed in the fuselage or in dedicated volumes, because their geometry, insulation thickness and pressure-vessel requirements make wing storage difficult for transport configurations. The resulting integration problem affects the fuselage layout, usable cabin length, cargo capacity, operating empty weight, centre-of-gravity evolution and reserve strategy. Aircraft-level design studies have shown that liquid hydrogen storage trades are therefore strongly configuration-dependent and that tank sizing cannot be separated from mission and payload assessment [15–18]. Retrofit-oriented investigations are useful in this context because they provide a controlled way to quantify the penalties of introducing hydrogen into an existing or reference airframe, following the system-integration strategy of already designed reference aircraft [19–21]. Nevertheless, a retrofit approach necessarily limits the degrees of freedom available to the designer.

The main limitation of retrofit-based studies is that the airframe is often treated as already defined. The external geometry, aerodynamic sizing, wing area, wing loading, structural arrangement, propulsion installation and part of the internal layout are kept fixed, while the hydrogen system is accommodated inside the remaining volume and mass margins. This is justified in early feasibility studies and provides valuable information on payload-range trade-offs. However, it may conceal part of the actual potential of hydrogen-powered aircraft. If the hydrogen system substantially changes payload, fuel mass and take-off weight, an aircraft inherited from a kerosene design may operate far from the optimal point for which its lifting system, structural layout and aerodynamic performance were originally optimized. A more informative conceptual-design process should therefore allow the airframe, the hydrogen storage system and the mission requirements to adapt to each other from the beginning of the design loop.

This need becomes more evident when unconventional aircraft configurations are considered. Alternative architectures are often investigated because they can offer aerodynamic, structural or volumetric opportunities that are not available within the classical tube-and-wing paradigm. Reviews of joined-wing and unconventional civil-aircraft concepts have highlighted the design potential of architectures able to redistribute volume and lifting surfaces in a less conventional manner [22–24]. Among these concepts, the box-wing configuration is of particular interest for medium-range transport applications [25]; an example of this configuration is reported in Figure 1. Its joined lifting system is based on Prandtl's Best Wing System theory: for fixed lift and span, an appropriate distribution of lift on the horizontal wings and on the vertical tip wings can reduce induced drag, with the lift on horizontal wings resulting from the superposition of constant and elliptical components and a butterfly-shaped form for the vertical wing tips [26–29]. This architecture can therefore provide high span efficiency, especially under airport-span constraints, while the presence of two staggered lifting surfaces can efficiently support different load distributions and larger fuselage concepts. For liquid-hydrogen aircraft, its interest is not limited to aerodynamic efficiency. The architecture can also provide functional flexibility in fuselage integration and internal-volume allocation, which are critical aspects for cryogenic tank integration [30].



Figure 1 – Illustrative box-wing aircraft configuration used to clarify the reference architecture discussed in the present work.

The content of this paper is an incremental contribution based on previous preliminary research addressing the study of the retrofitting of hydrogen-based aircraft. A first study developed a parametric methodology for the conceptual fuselage integration of non-integral liquid hydrogen tanks in short-medium range aircraft, with attention to tank geometry, structural sizing, insulation, hydrogen thermodynamics, boil-off, venting and mission simulation [31]. The approach was then applied to both tube-and-wing reference aircraft, also in relation to publicly available reference-aircraft datasets [32], and to a medium-range liquid-hydrogen-powered box-wing aircraft, where it enabled a preliminary performance analysis of passenger capacity, tank volume and achievable range [33]. Those studies were necessary to identify the dominant integration mechanisms and to quantify the implications of replacing kerosene storage with liquid hydrogen tanks. At the same time, they retained a predominantly retrofit perspective. The aircraft geometry and several design assumptions were inherited from previously defined configurations, and the airframe was not allowed to fully co-evolve with the hydrogen storage system.

The research gap addressed in the present paper is therefore methodological. The objective is to move from the assessment of hydrogen integration in a largely predefined aircraft toward a fully parametric and integrated conceptual design workflow in which geometry, aerodynamics, mass estimation, liquid-hydrogen tank sizing, mission performance, tank thermodynamics, reserve requirements and maximum take-off weight are solved within a coupled iterative process. The focus is not on providing a final optimized aircraft, but on establishing a transparent and reproducible conceptual framework that can be used to explore aircraft of any configuration. In this work, the box-wing architecture is used as the reference application because it enables direct comparison with previous retrofitting studies by the authors. Within this framework, the tank system is not treated as a secondary installation constraint, but as a design element that affects payload, range, mass breakdown, volume allocation and mission feasibility.

The paper is organized as follows. Section 2 presents the proposed conceptual design methodology, including the parametric implementation, aircraft geometry model, aerodynamics and propulsion modelling, mass estimation, liquid-hydrogen tank sizing, coupled mission and thermodynamic simulation, reserve treatment and maximum take-off weight convergence. Section 3 reports the numerical application of the workflow, including the demonstration convergence case, the reference box-wing liquid-hydrogen family, a redesign-aware wing-area variation, tank structural and cryogenic-storage effects, cross-class applicability and the preliminary parametric dataset generated for optimization-oriented studies. Finally, Section 4 presents the concluding remarks and summarizes the main findings of the study, highlighting the key outcomes and potential directions for future research.

2. Methodology

2.1 Design Rationale and Problem Definition

The methodology proposed in this work is an aircraft-level conceptual design workflow for liquid hydrogen-powered aircraft. Its objective is not to assess whether cryogenic tanks can be inserted into a pre-existing fuselage, but to resolve the coupled design problem generated by the simultaneous presence of an assigned aircraft architecture and a liquid-hydrogen storage system. The workflow integrates aircraft geometry, aerodynamic database generation, mass estimation, tank sizing, tank thermal-state evaluation, mission performance assessment, reserve requirement determination, payload accommodation, and maximum take-off weight convergence into a unified computational

framework.

This formulation is motivated by a limitation of retrofit-oriented studies. In a retrofit process, the airframe is usually inherited from a kerosene-powered reference aircraft: external geometry, wing area, wing loading, aerodynamic polar, structural layout, cabin arrangement and part of the mission definition remain fixed, while the hydrogen system is accommodated within the available volume. This approach is valuable as a preliminary feasibility step and was adopted in previous investigations on liquid hydrogen aircraft and on box-wing configurations [31, 33]. However, it may become restrictive when hydrogen is treated as an add-on rather than as a design driver. Liquid hydrogen has high gravimetric energy density but low volumetric energy density; it also requires cryogenic storage, insulation, ullage volume, pressure relief, non-negligible tank mass and suitable integration with the fuselage. These requirements affect the payload layout, cargo capability, operating empty weight, fuel availability, reserve margin and achievable range. If the airframe remains unchanged while payload and take-off weight change significantly, the resulting aircraft may operate away from the aerodynamic and structural optimum for which it was originally designed.

The present workflow therefore treats the hydrogen storage system as part of the aircraft-level sizing consistency process. For a prescribed set of top-level requirements and independent design variables, the code generates the aircraft geometry, evaluates the aerodynamic data required by the mission analysis routine, estimates the aircraft mass breakdown, sizes the liquid-hydrogen tanks, simulates the mission together with the tank thermal state, and iterates until the maximum take-off weight is consistent with the computed empty mass, payload, tank dry mass and initial hydrogen mass. The tool is intended for conceptual design studies and parametric analyses, and can be integrated in optimization frameworks.

The design process is initialized from a centralized input structure. The input defines aircraft geometry, aerodynamic settings, mass-model assumptions, tank parameters, thermal-model parameters, mission requirements and convergence options. The main design variables include front- and rear-wing planform data, wing relative placement, twist distributions, fuselage length and characteristic cross-section dimensions, vertical-tail data, propulsion-installation data and cabin-layout information. The tank-related design variables include tank radius, cylindrical length, number and arrangement of tank groups, radial clearance, endcap aspect ratio, insulation thickness or insulation policy, fill factor, venting pressure, design pressure and support-distance assumptions. The mission inputs include cruise Mach number, cruise altitude, climb programme, time-step settings, diversion distance, holding requirements and reserve policy. In the present implementation, the nominal range can be treated as a fuel-limited output rather than as a fixed prescribed value. The automatic routine then searches for the maximum feasible nominal range compatible with the liquid-hydrogen mass, boil-off, venting and reserve requirements.

2.2 Parametric, modular and configuration-agnostic implementation

The workflow is organized as a fully parametric conceptual design environment. The aircraft is defined by independent input variables and derived quantities that are propagated through geometry generation, aerodynamic analysis, mass estimation, tank sizing, mission simulation and maximum take-off weight convergence. For an assigned design vector, the routine returns a self-consistent aircraft state; the same computational core can therefore be used for sensitivity analyses and can be integrated in optimization frameworks.

The implementation is also modular, and the disciplinary blocks exchange aircraft-level quantities through explicit interfaces, so that individual models can be replaced when more appropriate data are available. For instance, the semi-empirical structural-mass estimates used in the present implementation may be substituted by surrogate models derived from higher-fidelity structural analyses, while preserving the same global consistency logic. Although the paper focuses on a box-wing aircraft, the workflow is not intrinsically limited to this architecture. Tube-and-wing or other non-conventional configurations can be treated by providing consistent geometric, aerodynamic, mass and tank-integration parameters. This configuration-agnostic capability constitutes the computational backbone of the method; however, the validity of each disciplinary model must still be evaluated for the specific aircraft class under consideration.

2.3 Aircraft geometry and box-wing architectural variables

The geometrical model is based on a parametric representation of the aircraft. In the box-wing application considered here, the front and rear wings are described as distinct lifting surfaces, while the lateral connection of the lifting system is represented by vertical tip wings connecting the front and rear tips.

The box-wing architecture is relevant to the present hydrogen problem for aerodynamic and volumetric reasons. Its joined lifting system may reduce induced drag under span constraints when the lift distribution over the horizontal wings and the vertical tip wings is selected consistently with Best Wing System theory. In previous box-wing studies, this feature was mainly exploited to increase passenger capacity and to remain compatible with airport-span limits. In a liquid-hydrogen aircraft, the same internal-volume flexibility becomes a design resource because cryogenic tanks compete directly with cabin and cargo volume.

Fuselage length and cross-section affect aerodynamic drag, mass estimates and the space available for full-section internal tanks. When a full-section tank is installed (i.e., a tank whose external surface is tangent to the fuselage cross section), the tank longitudinal span removes usable cabin and cargo length. Consequently, the passenger count, payload, cabin crew complement, and container-carrying capability are updated consistently rather than being specified independently. In the present implementation, this automatic cabin-fuselage-tank sizing consistency is focused on full-section tank intrusion. Partial-section tank layouts are recognized as relevant extensions because they may preserve part of the passenger cabin or cargo deck at the cost of reduced hydrogen volume; hence this model will be implemented in future extensions of the framework. Figure 2 illustrates the fuselage-section layout used to distinguish full-section (FS) and partial-section (PS) cryogenic tank integration.

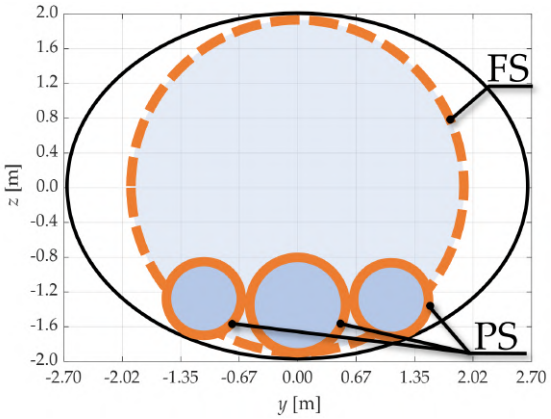


Figure 2 – Illustrative fuselage-section layout used to discuss full-section (FS) and partial-section (PS) cryogenic tank integration inside the passenger/cargo volume.

2.4 Aerodynamics and propulsion module

The aerodynamics and propulsion module supplies the mission routine with the data required to evaluate the aircraft state along the trajectory. The aerodynamic part is computed with methods and tools suitable for the conceptual design stage. For each prescribed geometry and flight condition, a vortex-lattice solution is generated, profile and parasite drag increments are added, and a wave-drag correction is included when required. The database is organized in terms of Mach number, altitude and lift coefficient, and it returns the drag coefficient, lift-to-drag ratio and angle of attack required by the subsequent mission time-marching calculation. In practical terms, the database acts as a flight-condition lookup table for the mission routine: each point required by the trajectory integration is obtained by interpolation within the precomputed Mach-altitude-lift-coefficient domain. When the external geometry is changed by an outer design iteration, the aerodynamic database is regenerated; during a single maximum take-off weight convergence run, the geometry is fixed and the same database is reused while the aircraft mass and operating lift coefficient evolve.

For each database point, the total drag coefficient is computed as

$$C_D = C_{D,i} + C_{D,0} + C_{D,\text{wave}}, \tag{1}$$

where $C_{D,i}$ is the inviscid vortex-lattice contribution, mainly associated with lift-dependent drag and the load distribution computed by means of the solver AVL; $C_{D,0}$ is the sum of viscous profile and parasite contributions; and $C_{D,\mathrm{wave}}$ is the compressibility correction. The zero-lift, viscous and parasite term is decomposed as

$$C_{D,0} = C_{D,\mathrm{fus}} + C_{D,\mathrm{ups}} + C_{D,\mathrm{fw}} + C_{D,\mathrm{rw}} + C_{D,\mathrm{tip}} + C_{D,\mathrm{fin}} + C_{D,\mathrm{nac}}. \tag{2}$$

The terms on the right-hand side denote, respectively, fuselage friction and form drag, aft-body upsweep drag, front-wing profile drag, rear-wing profile drag, tip-wing profile drag, vertical-tail drag and nacelle drag. The fuselage and nacelle increments are evaluated through turbulent skin-friction correlations with form and interference factors [35].

The lifting-surface profile drag is obtained by spanwise integration of two-dimensional airfoil polar data over the front wing, rear wing and tip wings. For a generic lifting surface w, this contribution can be written in compact form as

$$C_{D,w} = \frac{1}{S_{\mathrm{ref}}} \sum_{p \in \mathscr{P}_w} \int_{y_p}^{y_{p+1}} c_p(y) c_{d,2D}\left(\alpha + \theta_p(y) + i_w\right) dy, \tag{3}$$

where S_{ref} is the aircraft reference area, p is the panel index, $\mathscr{P}_w$ is the set of panels of surface w, y_p and y_{p+1} are the inboard and outboard panel coordinates, $c_p(y)$ is the local chord, $c_{d,2D}$ is the airfoil drag coefficient interpolated from the selected polar, α is the aircraft angle of attack, $\theta_p(y)$ is the local twist and i_w is the incidence of the lifting surface.

The wave-drag correction is computed separately for the lifting surfaces specified in the aerodynamic settings. For each lifting surface s belonging to the set $\mathscr{S}_{\mathrm{wave}}$, the lift coefficient recovered from the vortex-lattice surface forces is first converted from aircraft-reference-area normalization to local surface-area normalization,

$$C_{L,s}^{\mathrm{surf}} = C_{L,s}^{S_{\mathrm{ref}}} \frac{S_{\mathrm{ref}}}{S_s}. \tag{4}$$

The drag-divergence Mach number is then estimated through a Korn-type relation,

$$M_{dd,s} = \frac{K_{A,s}}{\cos\Lambda_s} - \frac{(t/c)_s}{\cos^2\Lambda_s} - \frac{C_{L,s}^{\mathrm{surf}}}{10\cos^3\Lambda_s}, \tag{5}$$

where S_s is the planform area of surface s, $K_{A,s}$ is the airfoil technology factor, $(t/c)_s$ is the thickness-to-chord ratio and Λ_s is the sweep angle used for the correction. The critical Mach number is

$$M_{\mathrm{crit},s} = M_{dd,s} - \left(\frac{0.1}{80}\right)^{1/3}, \tag{6}$$

and the wave contribution of the surface is

$$C_{D,\mathrm{wave},s} = 20\max(M - M_{\mathrm{crit},s}, 0)^4. \tag{7}$$

The aircraft wave-drag correction is finally

$$C_{D,\mathrm{wave}} = \sum_{s \in \mathscr{S}_{\mathrm{wave}}} C_{D,\mathrm{wave},s}. \tag{8}$$

This implementation avoids using the total aircraft lift coefficient as a surrogate for the local lift of each wing and keeps the dependence on surface loading explicit.

The propulsion system-related part of the module is treated at conceptual level through the installed thrust-to-weight ratio, T/W. The mission routine can use a prescribed value of T/W or a value obtained from a conventional matching-chart calculation in the T/W–W/S plane, where W/S is the design wing loading. The active constraints may include take-off, climb, cruise and ceiling requirements, evaluated with the same aerodynamic drag polar and mass state used in the mission analysis. The resulting thrust loading is then passed to the aircraft-level sizing and mission modules. This step defines the installed thrust required by the aircraft, but does not replace a detailed hydrogen engine-cycle or heat-exchanger design.

2.5 Mass estimation module

The mass estimation module provides the operating-empty-weight estimate associated with the current aircraft geometry, passenger layout, installed propulsion characteristics and design range. It is intentionally separated from the tank-sizing module. Airframe, propulsion, systems, furnishing and operating items are evaluated by a FLOPS-inspired conceptual mass core [36], while the cryogenic tank dry mass and liquid-hydrogen mass are computed separately and added later in the maximum take-off weight calculation routine.

The module receives the initial guess of sizing mass, front- and rear-wing geometry, fuselage dimensions, vertical-tail and tip-wing data, passenger and crew numbers, engine count, installed thrust, design range and service-level assumptions. The front and rear wings are evaluated separately rather than being collapsed into a single equivalent wing. Their estimates depend on standard conceptual drivers such as lifting-surface area, span, aspect ratio, taper ratio, sweep, thickness-to-chord ratio, ultimate load factor and technology correction factors. For a box-wing, this is a potentially penalizing but conservative approximation, as proposed and discussed in Ref. [34]: the two horizontal wings are treated as conventional cantilever lifting surfaces, rather than as part of a single hyperstatic joined lifting system connected through the fuselage and tip wings, which could offer structural-mass reduction potential. The fuselage, propulsion installation and aircraft systems are treated consistently with transport-aircraft semi-empirical correlations, while selected operating items are updated from passenger, crew and cargo quantities. These relationships are used as conceptual correlations, not as detailed structural or systems design models.

The resulting contributions are grouped into structural, propulsion, systems, furnishing and operating mass groups. The manufacturer's empty weight and operating empty weight are obtained as

$$m_{\mathrm{MEW}} = 1.02\,(m_{\mathrm{STR}} + m_{\mathrm{PWR}} + m_{\mathrm{SYS}} + m_{\mathrm{FUR}}), \qquad m_{\mathrm{OEW}} = m_{\mathrm{MEW}} + m_{\mathrm{OP}}, \tag{9}$$

where m_{STR}, m_{PWR}, m_{SYS}, m_{FUR} and m_{OP} denote the structural, propulsion, systems, furnishing and operating mass groups, respectively. The factor 1.02 is retained as a conventional contingency factor on the manufacturer-empty-weight core. The tank dry mass and the initial hydrogen mass do not enter Eq. (9); they are used separately in the aircraft-level mass consistency calculation.

2.6 Liquid hydrogen tank sizing and aircraft-level integration

Figure 3 summarizes the tank geometry and two-phase hydrogen state used by the storage-system model before the governing sizing equations are introduced.

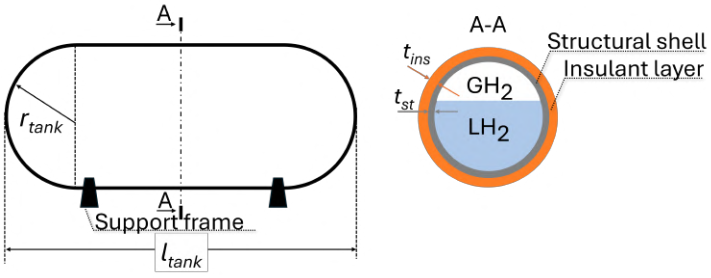


Figure 3 – Conceptual tank model with cylindrical pressure-vessel geometry, ellipsoidal endcaps, external insulation, support-frame idealization and two-phase liquid/gaseous hydrogen state.

The storage system is represented by non-integral cylindrical pressure vessels with ellipsoidal endcaps and an external foam-based insulation layer represented through temperature-dependent foam properties. This modelling choice is consistent with the conceptual level of the present work and with previous hydrogen integration studies [31]. Integral tanks, conformal tanks and detailed local structural integration are not included. The tank module nevertheless provides more than volume capacity: it computes internal volume, initial hydrogen mass, pressure-vessel wall thickness, insulation mass, dry tank mass and the structural checks used to verify the conceptual feasibility of the tank design.

For each design case, the tank-sizing layer resolves the available fuselage section from the selected integration assumptions (as the tanks considered in this study are non-integral with the fuselage

structure). For the sake of simplicity, the present application uses a full-section tank group and evaluates the tank radius from the available fuselage envelope after applying the prescribed clearance. Repeated tank groups can be expanded into physical tanks before mass and capacity aggregation, so that the same sizing logic applies to all tanks generated by the layout module.

For a generic tank, the foam external radius is R_f, the structural external radius is R_s, the cylindrical length is L, and the endcap aspect ratio is h_e. The insulation thickness is $t_{\text{ins}} = R_f - R_s$. The cylindrical shell thickness is t_c and the endcap thickness is t_e. The internal shell radius R_i and the internal endcap R_e equivalent radius are

$$R_i = R_s - t_c, \qquad R_e = R_s - t_e. \tag{10}$$

The internal tank volume V_{int} is obtained as the sum of the cylindrical volume and the two semi-ellipsoidal heads,

$$V_{\text{int}} = \pi R_i^2 L + \frac{4}{3}\pi R_e^3 h_e. \tag{11}$$

The initial liquid hydrogen mass $m_{\text{LH2,0}}$ is

$$m_{\text{LH2,0}} = \phi_{\text{fill}} V_{\text{int}} \rho_{\text{LH2,ref}}, \tag{12}$$

where ϕ_{fill} is the liquid fill factor and $\rho_{\text{LH2,ref}}$ is the reference liquid-hydrogen density used by the thermal model. The remaining internal volume initializes the gaseous ullage.

The structural sizing uses an ASME-inspired pressure-vessel backbone, following the design-by-rule philosophy adopted in the ASME Boiler and Pressure Vessel Code for pressure-vessel calculations [37]. The allowable stress σ_{all} is defined as

$$\sigma_{\text{all}} = \min\left(\frac{\sigma_y}{FS_y}, \frac{\sigma_u}{FS_u}\right), \qquad \sigma_w = \eta_w \sigma_{\text{all}}, \tag{13}$$

where σ_y and σ_u are the yield and ultimate strengths at cryogenic temperature, FS_y and FS_u are the corresponding pressure-sizing safety factors, η_w is the welding efficiency and σ_w is the weld-corrected allowable stress. The pressure-driven cylindrical t_c and endcap t_e thickness estimates are

$$t_c = \max\left[t_{\min}, \frac{p_d R_i}{\sigma_{\text{all}}\eta_w - 0.6p_d}, \frac{0.5 p_d R_i}{\sigma_{\text{all}}\eta_w + 0.2p_d}\right], \tag{14}$$

$$t_e = \max\left[t_{\min}, \frac{k_e p_d R_e}{\sigma_{\text{all}}\eta_w - 0.1p_d}\right], \qquad k_e = \frac{2 + h_e^{-2}}{6}. \tag{15}$$

Here p_d is the design pressure, $t_{\min}$ is the enforced minimum wall thickness and k_e is the ellipsoidal-head shape factor. These equations provide the pressure-driven starting point. The thickness of the cylindrical wall is then increased, if necessary, until the combined manoeuvre-load and buckling checks are satisfied.

The structural volume V_{str} and insulation volume V_{ins} are evaluated as

$$V_{\text{str}} = \pi\left(R_s^2 - R_i^2\right)L + \frac{4}{3}\pi\left(R_s^3 - R_e^3\right)h_e, \tag{16}$$

$$V_{\text{ins}} = \pi\left(R_f^2 - R_s^2\right)L + \frac{4}{3}\pi\left(R_f^3 - R_s^3\right)h_e, \tag{17}$$

so that the corresponding structural mass m_{str}, insulation mass m_{ins} and filled tank mass m_{filled} are

$$m_{\text{str}} = \rho_{\text{str}} V_{\text{str}}, \qquad m_{\text{ins}} = \rho_{\text{ins}} V_{\text{ins}}, \qquad m_{\text{filled}} = m_{\text{str}} + m_{\text{ins}} + m_{\text{LH2,0}}. \tag{18}$$

In Eq. (18), ρ_{str} and ρ_{ins} are the structural-material and insulation densities, respectively, and m_{filled} is the mass of the tank including structure m_{str}, insulation m_{ins} and initial liquid hydrogen used in the inertial-load checks.

The combined-load verification is applied to the cylindrical shell. Its annular area A_c and bending inertia I_c are

$$A_c = \pi\left(R_s^2 - R_i^2\right), \qquad I_c = \frac{\pi}{4}\left(R_s^4 - R_i^4\right). \tag{19}$$

For prescribed vertical and axial load factors n_z and n_x, the equivalent vertical load F_z, bending moment M_b and axial force F_x are approximated as

$$F_z = n_z m_{\text{filled}} g_0, \qquad M_b = \frac{F_z d_s}{8}, \qquad F_x = n_x m_{\text{filled}} g_0, \tag{20}$$

where g_0 is standard gravity and d_s is the support distance. The bending σ_b and axial stresses σ_x are

$$\sigma_b = \frac{M_b R_s}{I_c}, \qquad \sigma_x = \frac{F_x}{A_c}. \tag{21}$$

The pressure stresses are

$$\sigma_\theta = \frac{p_d R_i}{t_c} + 0.6 p_d, \qquad \sigma_{p,l} = \frac{1}{2}\frac{p_d R_i}{t_c} - 0.2 p_d, \tag{22}$$

where σ_θ is the hoop stress and $\sigma_{p,l}$ is the longitudinal pressure stress. The tensile σ_{ten} and compressive σ_{comp} stresses used in the final checks are

$$\sigma_{\text{ten}} = \sigma_{p,l} + \sigma_b, \qquad \sigma_{\text{comp}} = \sigma_x + \sigma_b. \tag{23}$$

The shell is considered consistent with the design parameters if

$$\sigma_\theta \le \sigma_w, \qquad \sigma_{\text{ten}} \le \sigma_w, \qquad \sigma_{\text{comp}} \le \sigma_{\text{buck}}. \tag{24}$$

The buckling allowable σ_{buck} is written as

$$\sigma_{\text{buck}} = \frac{F_{ba}}{FS_b}, \tag{25}$$

where F_{ba} is the ASME-inspired cylindrical-shell allowable selected for the applicable shell regime and FS_b is the buckling safety factor.
If the pressure-only estimate does not satisfy Eq. (24), the cylindrical thickness is increased by bisection. At each bisection step the geometry, tank masses, inertial loads, stresses and buckling margin are recomputed. This is required because increasing thickness improves stress margins but also increases structural mass and therefore the inertial loads. After all physical tanks have been sized, the aircraft-level tank masses are obtained as

$$m_{\text{tank,str}} = \sum_j m_{\text{str},j}, \qquad m_{\text{tank,ins}} = \sum_j m_{\text{ins},j}, \qquad m_{\text{tank,dry}} = m_{\text{tank,str}} + m_{\text{tank,ins}}, \tag{26}$$

where j spans all physical tanks. The tank dry mass and the initial hydrogen mass are used to calculate the maximum take-off weight. The integration module then updates the passenger capacity, payload, cabin crew and cargo/container capability according to the tank longitudinal intrusion in the full-section layout.

2.7 Integrated mission and hydrogen thermodynamic simulation

The mission and tank thermal analyses are performed in a coupled time-marching framework. Figure 4 summarizes the computational sequence used to connect aircraft selection, tank definition, mission performance analysis and range calculation. This is one of the central elements of the methodology. At each time step, the mission routine evaluates the aircraft aerodynamic and propulsive state, while the tank module determines the liquid hydrogen actually available to the engines, the heat-induced phase change and any gaseous hydrogen expelled by the pressure-relief system. The mission is therefore not reduced to a static fuel fraction or to an isolated segment-wise energy balance.
The mission profile includes ground hold after liquid-hydrogen loading, taxi, take-off, climb, cruise, descent and a reserve sequence including diversion and holding. Diversion is represented by an editable route distance, while holding is represented by a specified duration at a prescribed low-altitude condition. Holding is intended to consume fuel and time but does not increase the nominal

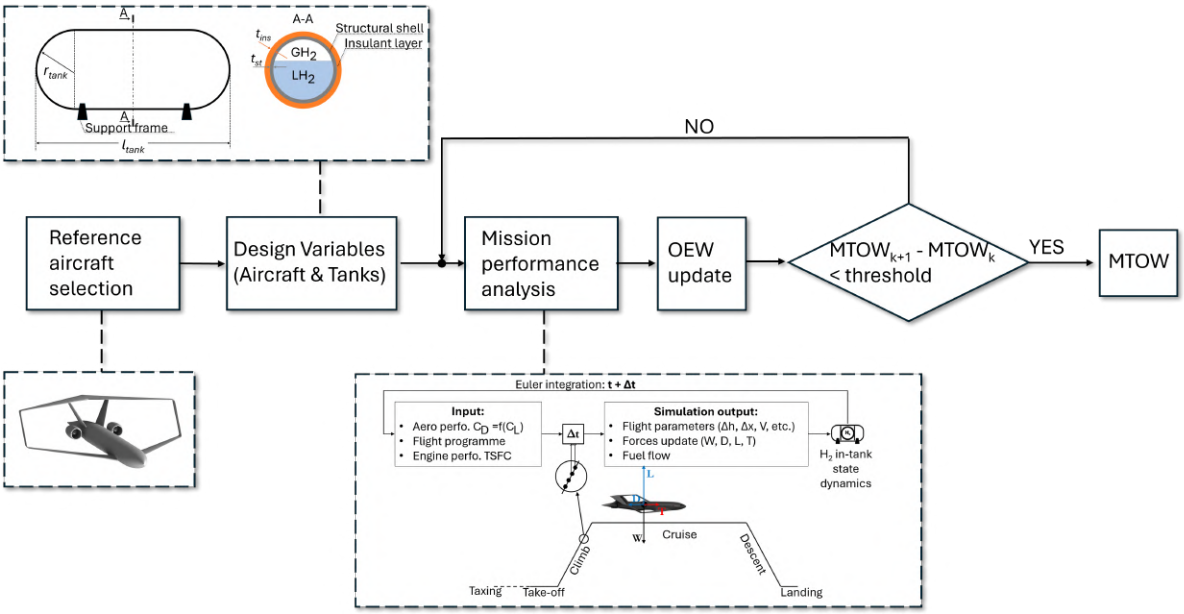


Figure 4 – Workflow for the conceptual design of LH2-based aircraft.

range. The holding Mach number may be prescribed or selected from the aerodynamic database by minimizing quasi-steady fuel flow at the selected holding altitude.

The aircraft is modelled as a point mass in the vertical plane. The equations of motion are integrated by an explicit step-by-step iteration over the prescribed mission schedule. At the beginning of each time step, altitude, Mach number, aircraft mass and segment target are known. The current mass fixes the required lift coefficient; the aerodynamic database provides drag and angle of attack; the point-mass force balance gives the thrust required for climb, cruise or descent; and the propulsion model converts this thrust into a hydrogen demand. The tank routine then determines the hydrogen actually drawn and vented over the same interval. These quantities update the aircraft mass and tank state, which become the initial conditions for the next time step. This iterative marching procedure is repeated until the segment target is reached or until a stopping criterion is triggered. For an airborne time step, the true airspeed V and dynamic pressure q are

$$V = Ma(h), \qquad q = \frac{1}{2}\rho(h)V^2, \tag{27}$$

where $a(h)$ and $\rho(h)$ are the speed of sound and density at altitude h. The required lift coefficient C_L is

$$C_L = \frac{W}{qS_{\text{ref}}}, \qquad W = m_{\text{ac}} g_0, \tag{28}$$

where W is aircraft weight and m_{ac} is aircraft mass. The aerodynamic database is queried at (M, h, C_L) and the drag D is computed as

$$D = qS_{\text{ref}} C_D(M, h, C_L). \tag{29}$$

As hydrogen is burned or vented, m_{ac} changes, and the operating lift coefficient and drag are updated accordingly.

The required thrust T_{req} follows a simple point-mass balance. During climb, for a prescribed altitude rate $\dot{h} > 0$,

$$T_{\text{req}} = D + W\frac{\dot{h}}{V}. \tag{30}$$

During cruise and diversion cruise, level quasi-steady flight gives

$$T_{\text{req}} = D. \tag{31}$$

For descent, the descent force balance gives a point-mass thrust contribution

$$T_{\text{req}} = \max\left(0, D - W\frac{|\dot{h}|}{V}\right), \tag{32}$$

with an optional idle-thrust floor depending on the selected policy. Taxi, take-off and other low-speed phases are represented by prescribed fractions of installed maximum thrust or by explicit fuel-flow overrides, following the ICAO landing-and-take-off cycle logic used for standardized engine operating modes [38].

The engine hydrogen demand Δm_{dem} is obtained from a segment-dependent constant specific fuel consumption model,

$$\dot{m}_{\mathrm{H2,eng}} = c_j T_{\mathrm{req}}, \qquad \Delta m_{\mathrm{dem}} = \dot{m}_{\mathrm{H2,eng}} \Delta t, \tag{33}$$

where c_j is the specific fuel consumption of segment j, $\dot{m}_{\mathrm{H2,eng}}$ is the related hydrogen consumption per unit of time, and Δt is the time increment. This is a conceptual propulsion model: it does not solve the hydrogen turbofan cycle, heat-exchanger design, combustor behaviour or off-design engine performance. The aircraft mass m_{ac} updated at time step n is

$$m_{\mathrm{ac}}^{n+1} = m_{\mathrm{ac}}^{n} - \Delta m_{\mathrm{dem}} - \Delta m_{\mathrm{vent}}, \tag{34}$$

where Δm_{vent} is the gaseous hydrogen vented during the same step.

The thermal model is applied to each physical tank and then aggregated. At the start of the time step, the engine draw is distributed among active tanks according to the selected policy and limited by the liquid hydrogen mass above the minimum allowed residual mass. The heat leak into each tank is evaluated with a resistance network. The external area A_{ext} is approximated as the cylindrical area plus the area of an equivalent ellipsoid for the two endcaps. The conductive-convective heat input $\dot{Q}_{\mathrm{cc}}$ is

$$\dot{Q}_{\mathrm{cc}} = \max\left[0, \frac{T_\infty - T_{\mathrm{tank}}}{R_{\mathrm{ext}} + R_{\mathrm{ins}} + R_{\mathrm{int}}}\right], \tag{35}$$

where T_∞ is atmospheric temperature, T_{tank} is tank saturation temperature, R_{ext} is the external convective thermal resistance, R_{ins} is the insulation conductive thermal resistance and R_{int} is the internal convective thermal resistance. These resistances are defined as

$$R_{\mathrm{ext}} = \frac{1}{h_{\mathrm{ext}} A_{\mathrm{ext}}}, \qquad R_{\mathrm{ins}} = \frac{t_{\mathrm{ins}}}{k_{\mathrm{ins}} A_{\mathrm{ext}}}, \qquad R_{\mathrm{int}} = \frac{1}{h_{\mathrm{int}} A_{\mathrm{int}}}. \tag{36}$$

Here h_{ext} and h_{int} are external and internal heat-transfer coefficients, k_{ins} is insulation thermal conductivity and A_{int} is the internal heat-transfer area. The external coefficient is the larger of a natural-convection floor and a forced-convection estimate,

$$h_{\mathrm{ext}} = \max\left(h_{\mathrm{nat}}, \frac{Nu_D k_{\mathrm{air}}}{D_{\mathrm{tank}}}\right), \qquad D_{\mathrm{tank}} = 2R_f, \tag{37}$$

where h_{nat} is the natural-convection floor, Nu_D is the diameter-based Nusselt number and k_{air} is air thermal conductivity. Total heat leak $\dot{Q}$ is computed as follows

$$\dot{Q} = \dot{Q}_{\mathrm{cc}} + \varepsilon \sigma_{\mathrm{SB}} A_{\mathrm{ext}} \max\left(0, T_\infty^4 - T_{\mathrm{tank}}^4\right), \tag{38}$$

where ε is emissivity, and σ_{SB} is the Stefan-Boltzmann constant.

The operational tank model treats the hydrogen as a lumped two-phase system. Saturated liquid and gas properties are interpolated from cached tables as functions of pressure. For a tank at time step n, with liquid and gas masses m_l^n and m_g^n, the total hydrogen mass m^* after engine draw and before heat addition is

$$m^* = m_l^n - \Delta m_{\mathrm{dem}} + m_g^n. \tag{39}$$

The corresponding internal energy U^* before heat addition is

$$U^* = (m_l^n - \Delta m_{\mathrm{dem}})\, u_l(p^n) + m_g^n u_g(p^n), \tag{40}$$

where $u_l(p^n)$ and $u_g(p^n)$ are saturated liquid and gas specific internal energies at pressure p^n. After heat input, the updated internal energy U_{tar} is calculated as follows

$$U_{\mathrm{tar}} = U^* + \dot{Q}\Delta t. \tag{41}$$

For a saturation pressure p, the specific volume $\bar{v}$ (i.e., the ratio between the volume and the mass of a specific substance) fixes the vapor quality,

$$\bar{v} = \frac{V_{\text{tank}}}{m^*}, \qquad x(p) = \frac{\bar{v} - v_l(p)}{v_g(p) - v_l(p)}, \tag{42}$$

where V_{tank} is the internal tank volume, x is vapor quality, and v_l and v_g are saturated liquid and gas specific volumes. The pressure is obtained by solving

$$U(p) = m^* \left[(1 - x(p))u_l(p) + x(p)u_g(p)\right] = U_{\text{tar}}. \tag{43}$$

Eq. (43) accounts for the coupling among pressure, temperature, density, internal energy and vapor quality in saturated storage. If Eq. (43) would lead to a pressure above the venting pressure p_{vent}, the pressure-relief calculation is performed at $p = p_{\text{vent}}$. The vented phase is assumed to be gaseous hydrogen. The remaining mass m_f after venting satisfies

$$U_f(m_f) + (m^* - m_f)h_g(p_{\text{vent}}) = U_{\text{tar}}, \tag{44}$$

where h_g is saturated gas enthalpy at the venting pressure and U_f is the internal energy of the remaining two-phase hydrogen. The final vapor quality x_f is

$$x_f = \frac{V_{\text{tank}}/m_f - v_l}{v_g - v_l}, \qquad U_f = m_f \left[(1 - x_f)u_l + x_f u_g\right], \tag{45}$$

with all saturated properties evaluated at p_{vent}. The vented mass is then

$$\Delta m_{\text{vent}} = \max(0, m^* - m_f), \tag{46}$$

and the final gas and liquid masses are

$$m_g^{n+1} = m_f x_f, \qquad m_l^{n+1} = m_f(1 - x_f). \tag{47}$$

The boil-off mass recorded during the step is defined as the increase in gaseous hydrogen plus the gas removed by venting,

$$\Delta m_{\text{boil}} = \max\left[0, \left(m_g^{n+1} + \Delta m_{\text{vent}}\right) - m_g^*\right], \tag{48}$$

where m_g^* is the gas mass immediately after engine draw and before heat addition. This definition separates phase change from fuel loss. The coupled simulation stops if the fuel demand cannot be met, if the active tanks are depleted below the minimum liquid hydrogen mass, or if a pressure policy is violated. In fuel-limited range mode, the routine searches for the maximum nominal range that can be flown while completing the explicit reserve sequence and preserving the requested final liquid-hydrogen margin. The resulting range is therefore consistent with tank volume, heat leak, boil-off, venting, fuel draw, aircraft mass variation and reserve policy.

2.8 Maximum take-off weight convergence

The global converger resolves the maximum take-off weight for a prescribed design case. Starting from an initial guess, the current take-off mass is passed to the geometry, mass, tank and mission modules. The mass module computes m_{OEW}, the tank module computes $m_{\text{tank,dry}}$ and $m_{\text{LH2,0}}^{\text{tot}}$, the cabin sizing module updates payload and cargo quantities, and the mission-thermal solver evaluates the achievable range, fuel consumption, venting and reserve satisfaction.
The candidate take-off mass $m_{\text{TO,cand}}$ is

$$m_{\text{TO,cand}} = m_{\text{OEW}} + m_{\text{payload}} + m_{\text{tank,dry}} + m_{\text{LH2,0}}^{\text{tot}}, \tag{49}$$

where m_{payload} is the updated payload mass. The residual at iteration k is

$$r^{(k)} = m_{\text{TO,cand}}^{(k)} - m_{\text{TO,guess}}^{(k)}, \tag{50}$$

and the next guess is obtained through relaxed fixed-point iteration,

$$m_{\text{TO,guess}}^{(k+1)} = m_{\text{TO,guess}}^{(k)} + \omega r^{(k)}, \tag{51}$$

where ω is the relaxation factor. Convergence is accepted when the absolute and relative mass tolerances are satisfied and the mission-level checks are fulfilled. These checks may include positive finite range, absence of fuel shortfall, reserve satisfaction and a sufficient final liquid-hydrogen margin.

2.9 Methodological advancement over previous studies

The proposed methodology extends the authors' previous work by changing the role of the hydrogen system in the design process. The earlier integration study developed detailed parametric models for tank geometry, structural sizing, insulation, thermodynamics, venting and time-marching mission simulation, but the aircraft was treated through a retrofit perspective [31]. The subsequent aircraft-level study applied this logic to a medium-range architecture and highlighted the payload-range-volume trade-off of hydrogen-powered configurations [33]. In both cases, the analyses were useful for feasibility assessment, but the aircraft architecture remained largely inherited from a pre-existing reference design.

In the present workflow, tank integration is no longer only a constraint applied after the aircraft has been defined. Tank length affects passenger capacity and cargo. Tank volume affects initial hydrogen mass and fuel-limited range. Tank dry mass affects the take-off mass consistency process. Insulation affects boil-off and venting. Vented hydrogen affects useful fuel availability. Mission performance then feeds back into the mass convergence and into the systems design range. Aerodynamics, mass estimation, tank sizing, mission simulation, thermodynamics, reserves and maximum take-off weight are therefore treated as part of the same aircraft-level consistency problem. This makes the tool suitable for systematic exploration of hydrogen-powered aircraft families and provides a more consistent basis for future comparisons with reference concepts.

A specific risk addressed by this shift is the possibility of operating a large fraction of the mission away from the aerodynamic optimum of the original aircraft. Because liquid hydrogen has low volumetric density, tank accommodation can reduce payload and therefore maximum take-off weight. The resulting reduction in design wing loading may move the aircraft away from the lift-coefficient range for which the inherited lifting system was originally sized. A methodology in which airframe geometry, hydrogen volume, payload and mass convergence can adapt together is therefore needed before robust architectural conclusions are drawn.

2.10 Assumptions and limitations

The methodology is subject to assumptions that are acceptable at conceptual design level but must be considered when interpreting the results. The aerodynamic model is a medium-fidelity database approach and does not replace viscous CFD, detailed transonic analysis or high-lift assessment. Static stability, control authority and longitudinal trim are not implemented in the current convergence loop. Their introduction is the next natural development of the framework, because the AVL-based aerodynamic database already provides a suitable basis for preliminary stability and trim calculations [39].

The mass estimation module uses semi-empirical correlations and a simplified formulation for lifting system mass estimation; detailed structural sizing of the joined lifting system, fuselage frames, tank supports and load paths is not performed. Owing to the modular nature of the framework, each disciplinary model may be replaced by a higher-fidelity alternative, provided that it is wrapped through the same aircraft-level interfaces. For the structural sizing of box-wing lifting systems, this replacement could exploit FEM-based surrogate and metamodeling approaches already developed for early-stage box-wing design [40, 41].

The tank model includes pressure-vessel sizing, insulation mass and simplified inertial-load checks, but it does not represent detailed support frames, crashworthiness, local fuselage reinforcement, thermal stresses, fatigue, sloshing, emergency vent routing or certification-driven separation requirements. The automatic cabin, cargo and passenger sizing consistency is currently focused on full-section tank intrusion. Partial-section tank layouts, distributed tanks and more detailed cabin or cargo integration require additional rules before they can be resolved with the same consistency.

The thermal model is a lumped two-phase representation designed for robust iterative use. It includes heat leak, boil-off and venting, but it is not a high-fidelity cryogenic tank simulation. More detailed multiphase thermodynamics, stratification, active pressure control, thermal bridges, support heat leaks, multilayer insulation and spatially resolved tank-wall temperatures remain future refinements.

The propulsion model uses constant segment-level specific fuel consumption and simplified thrust assumptions. Engine cycle design, heat-exchanger sizing, combustor behaviour, nitrogen oxides

formation and off-design performance are not resolved.

3. Results and Discussion

The numerical results reported in this section are used to test the proposed workflow and to discuss the type of aircraft-level information that can be obtained when geometry, aerodynamic data, mass estimation, liquid-hydrogen tank sizing, mission simulation, tank thermodynamics, reserve requirements and maximum take-off weight convergence are treated within the same computational loop. The objective is not to identify a final optimized aircraft. The configurations are instead interpreted as demonstration points and controlled parametric variations. Accordingly, the discussion emphasizes mass-convergence behaviour, coupled aircraft-tank trends and modelling implications, rather than absolute design ranking.

For clarity, the main configurations are denoted by descriptive names throughout the section. The term *reference medium-range box-wing configuration* denotes the baseline box-wing family used to illustrate the effect of cylindrical tank length, namely the box-wing designed within the PARSIFAL project [30]. When a specific member of this family is required, it is identified by the corresponding cylindrical tank length, for example the *reference configuration with an 8 m cylindrical tank*. The term *reduced-wing-area variant* denotes the geometrically consistent case in which the same fuselage, tank arrangement, mission definition and reserve policy are retained, while the total reference wing area is reduced to two thirds of the reference value. Additional cases are described as regional-class, short-range, medium-range, long-range or airport-class box-wing configurations according to their aircraft-level role in the parametric campaign.

3.1 Demonstration case, MTOW convergence and mission-feasibility diagnostics

The first result concerns the numerical behaviour of the global converger. Figure 5 shows a representative convergence monitor produced during a full integrated run. The figure is included before any performance discussion because it illustrates a central feature of the methodology: the computed aircraft is not the output of an isolated range calculation, but the result of a coupled design consistency process involving mass, tank capacity, hydrogen mass, mission feasibility and reserve compliance.

The mass-convergence plot shows that the assumed take-off mass, the candidate mass reconstructed from the disciplinary modules, and the relaxed mass update progressively converge as the iterations proceed. The corresponding residual decreases toward the prescribed convergence tolerance. At each iteration, the aircraft mass affects the aerodynamic operating points, the fuel required by the mission, the tank state and the final reserve margin; the convergence history therefore provides a compact diagnostic of the complete aircraft-level design consistency. The mission/tank diagnostic graph connects this mass iteration to the residual hydrogen margin and to the computed nominal range, allowing the user to verify that the converged mass state is accompanied by satisfied mission and storage checks. The plot is therefore not intended to validate the aircraft concept; rather, it demonstrates that the workflow provides a transparent and traceable path from the input variables to a reserve-compliant aircraft state.

This point is particularly important for a medium-range aircraft retrofitted with fuselage-installed liquid-hydrogen tanks. When the cryogenic storage system is inserted into a configuration originally developed for conventional propulsion, the volumetric constraint imposed by the tank can strongly reduce the payload volume and the payload-related mass items. The resulting maximum take-off mass may then become substantially different from that of the conventional reference aircraft, with a detrimental cascade on wing loading, aerodynamic operating point and mission performance. The integrated workflow is designed to make this chain of consequences explicit, rather than treating the tank as a purely add-on component.

3.2 Reference box-wing LH2 configuration

The reference application is a medium-range box-wing aircraft equipped with full-section cylindrical liquid-hydrogen tanks inside the fuselage. The sketch of the planform of the reference configuration with an 8 m cylindrical tank is shown in Figure 6. The figure reports the box-wing layout, the longitudinal fuselage envelope, the tank location and the span constraint used in the comparison. This view

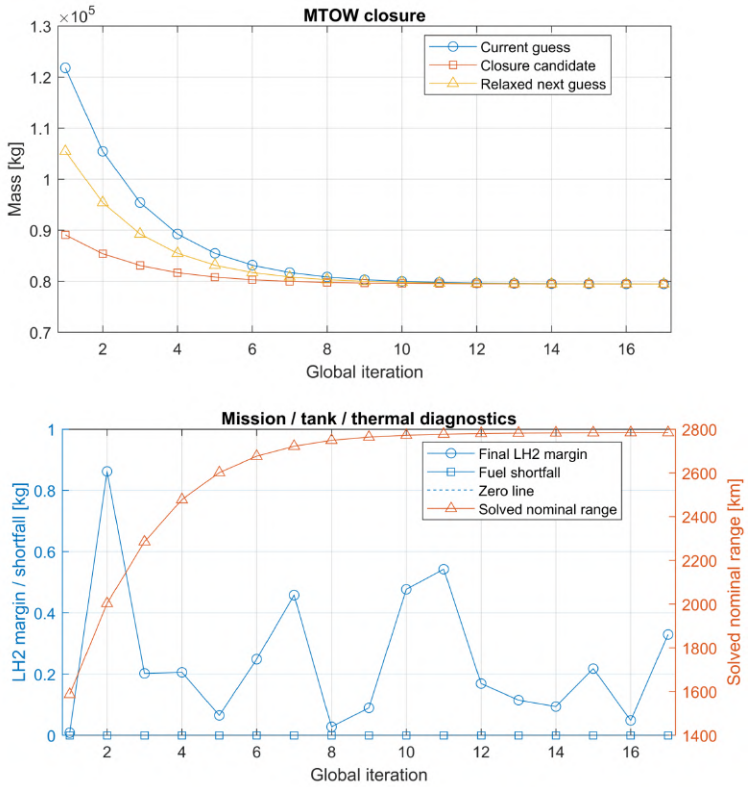


Figure 5 – Representative convergence monitor for the integrated workflow. The graphs track maximum take-off mass convergence and mission/tank-level diagnostics during the fixed-point iteration.

is useful because the results that follow are driven not only by aircraft mass or fuel capacity, but also by the volume occupied by the cryogenic storage system inside the fuselage.

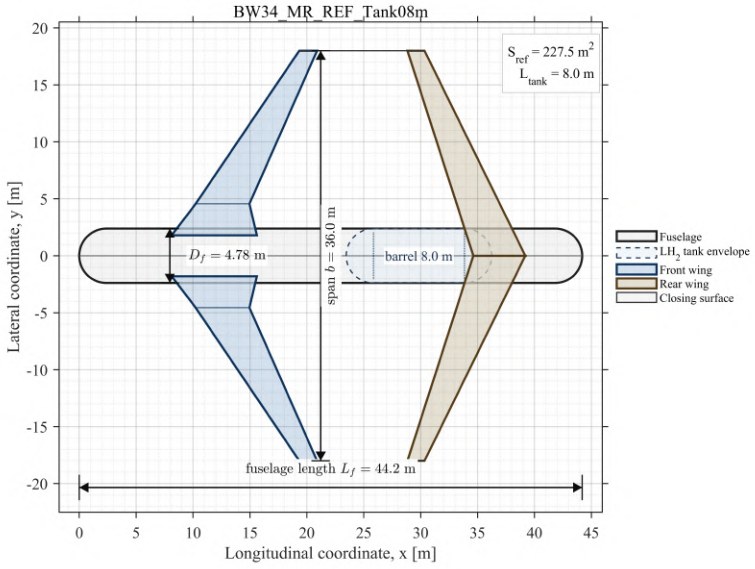


Figure 6 – Sketch of the planform of the reference medium-range box-wing configuration with an 8 m cylindrical liquid-hydrogen tank.

In this family, the cylindrical tank length is varied while the aircraft is updated by the workflow. Figure 7 shows the resulting nominal range as a function of tank length and also projects the same family on the passenger capacity–range plane. The trend is consistent with the expected role of tank volume: longer tanks increase the hydrogen mass and therefore extend the computed range. At the same time, the passenger capacity–range plane reveals that this extension is not obtained without a cabin-level consequence. As the full-section tank occupies more fuselage length, passenger

capacity decreases. The resulting trade is therefore not a single fuel-volume trend, but a coupled cabin-storage-mission trend.

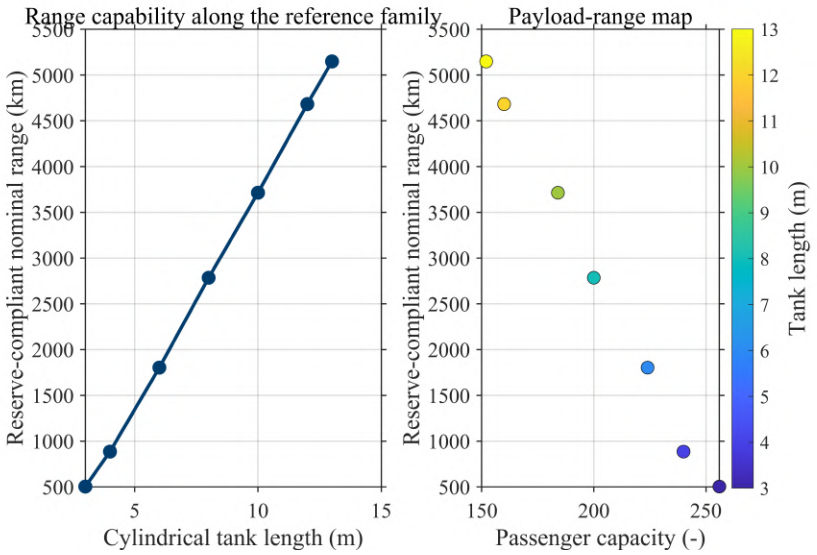


Figure 7 – Nominal range capability of the reference medium-range box-wing family as the cylindrical tank length is varied. The left graph shows the range trend with tank length, whereas the right graph maps the same cases in the passenger capacity–range plane.

Figure 8 complements the passenger capacity–range map by showing aircraft-level metrics associated with the same tank-length variation. The passenger capacity graph reflects the cabin penalty of full-section tank intrusion. The maximum take-off mass decreases across the family because the reduction in payload more than compensates for the increase in tank dry mass and hydrogen mass over the range considered. The fuel-tank capacity and tank-mass graphs show the expected increase in initial liquid-hydrogen mass and dry tank mass. The range and venting graphs indicate that the storage subsystem affects both the useful mission capability and the hydrogen lost through pressure management. The figure therefore illustrates why tank length cannot be treated as an isolated variable in a liquid-hydrogen conceptual design study: it propagates simultaneously into cabin accommodation, empty mass, tank mass, fuel inventory, range and venting.

The mass breakdown in Figure 9 provides the same interpretation in stacked form. The operating-empty-weight contribution, payload, tank dry mass and initial liquid-hydrogen mass are kept separate, following the mass-accounting definition introduced in the methodology. This separation is essential for the present application. A larger tank increases the onboard hydrogen and the dry tank penalty, but it can also reduce payload if the tank intrudes into the cabin. The total take-off mass is therefore an emergent result of the coupled design consistency process rather than an imposed scaling of the original aircraft. The plotted family makes this point explicit and confirms that the workflow can propagate a storage-layout choice up to the maximum take-off mass level.

The previous figures describe a reference family that retains the original lifting-surface area while adapting the liquid-hydrogen tank length. This is a useful first assessment, but it also exposes the limitation of a purely retrofit-like interpretation. If liquid-hydrogen integration and cabin accommodation reduce the converged take-off mass relative to the mass level for which the inherited lifting system was originally sized, the resulting wing loading may fall below the intended design value. The aircraft may then operate in a cruise lift-coefficient range that is not the most favourable for the inherited aerodynamic layout. To test this mechanism in a controlled way, a reduced-wing-area variant is generated. The fuselage, the 8 m tank, the reserve policy and the maximum span constraint are retained, whereas the total reference wing area is reduced from the reference value to two thirds, with the taper ratio and sweep angles preserved. Since the span is kept at the same value to exploit the 36 m upper bound associated with the ICAO Code C airport class [44], the aspect ratio of the reduced-area lifting system is higher than in the reference case. The corresponding planform is shown in Figure 10.

This reduced-wing-area case is not presented as an optimum. It is a redesign-aware variation used

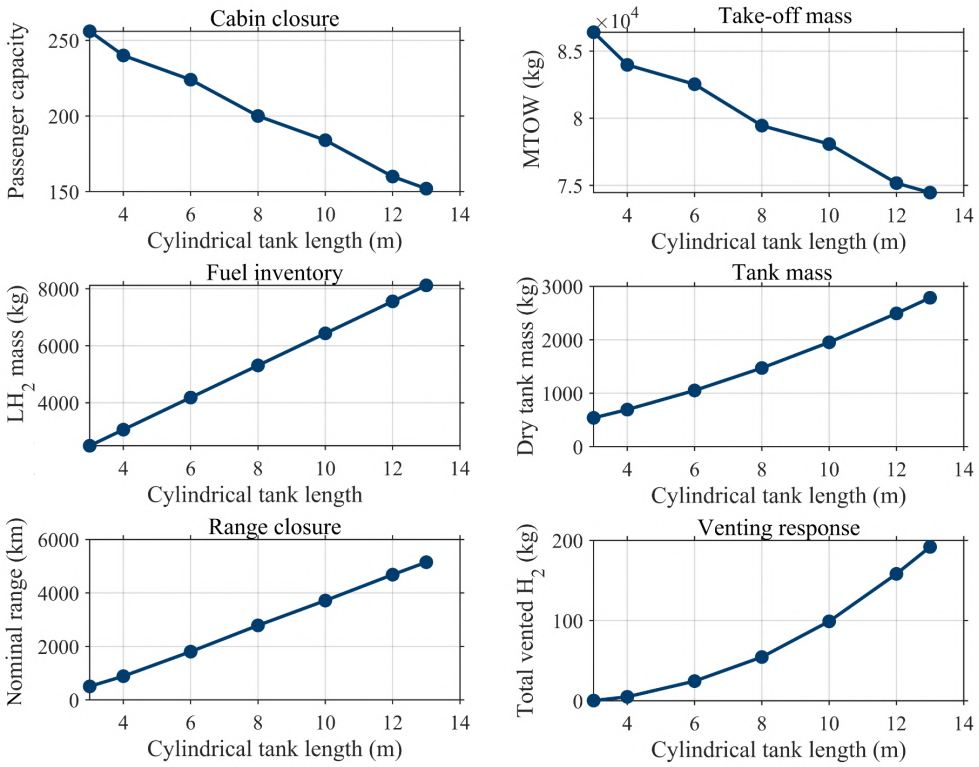


Figure 8 – Aircraft-level metrics for the reference medium-range box-wing family. The graphs report passenger capacity, maximum take-off mass, initial liquid-hydrogen mass, dry tank mass, nominal range and total vented hydrogen as functions of cylindrical tank length.

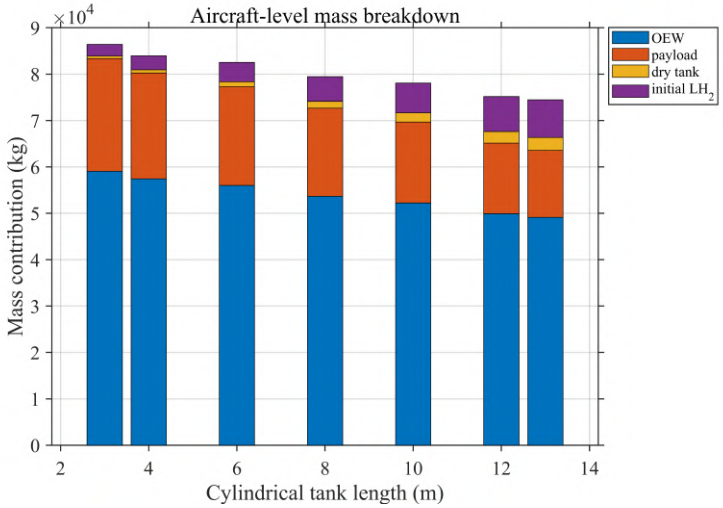


Figure 9 – Mass breakdown of the reference medium-range box-wing family for different cylindrical tank lengths.

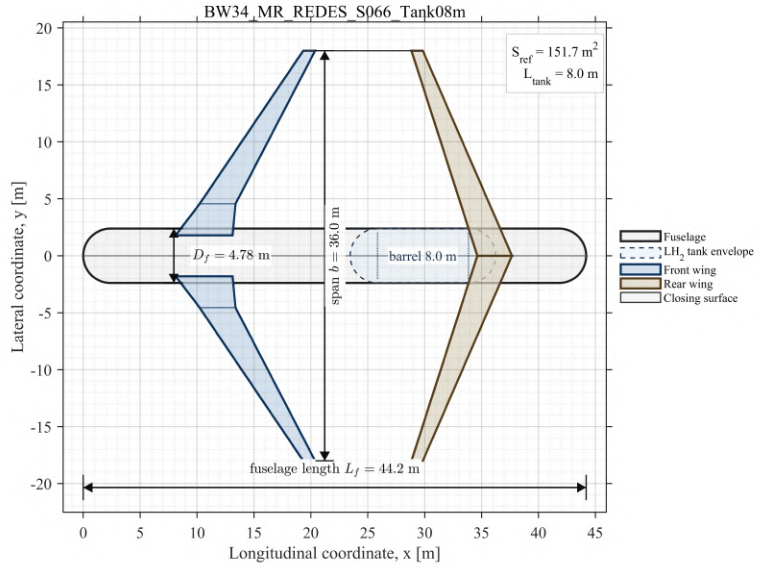


Figure 10 – Sketch of the planform of the reduced-wing-area medium-range variant with the same fuselage and 8 m cylindrical liquid-hydrogen tank as the reference case.

to distinguish two questions that would be mixed in a retrofit assessment: how much range is obtained from a given tank arrangement, and how the aircraft-level design consistency changes when the lifting-system area is adapted to the new mass level; it also provides a first test case for illustrating the parametric capability of the implemented workflow. Figure 11 compares the nominal range of the original and reduced-wing-area families over the same tank-length set. Across the plotted cases, the reduced-wing-area family gives a higher range than the reference family for the same tank length. The difference is moderate at the shortest tanks and becomes more visible as the storage capacity increases. This is consistent with the larger tank volume producing a stronger reduction of payload volume and hence a lower maximum take-off mass, so that the reference wing area becomes increasingly oversized for the updated liquid-hydrogen mass state. The reduced-area variant moves the aircraft toward a more favourable wing-loading and cruise-efficiency balance.

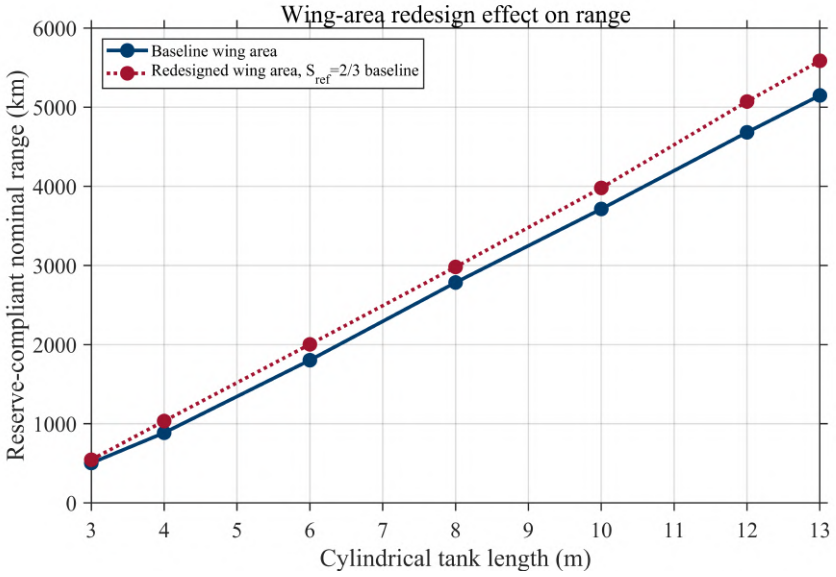


Figure 11 – Effect of a wing-area reduction on the nominal range. The two families have the same fuselage, tank lengths, tank arrangement and reserve policy; only the lifting-surface area and the aerodynamic performances differ.

The mechanism behind this trend is shown in Figure 12. The left-hand plot shows that the reduced-wing-area family exhibits higher wing loading across the tank-length range, as expected from the

smaller reference wing area. The right-hand plot shows that the average cruise lift-to-drag ratio is also higher for the reduced-wing-area family across the cases considered. This result should not be generalized beyond the present modelling assumptions, because it depends on the conceptual aerodynamic database and on the selected geometry-preserving area reduction. A liquid-hydrogen aircraft derived from a heavier baseline should not necessarily retain the original reference area without reassessing its cruise operating condition.

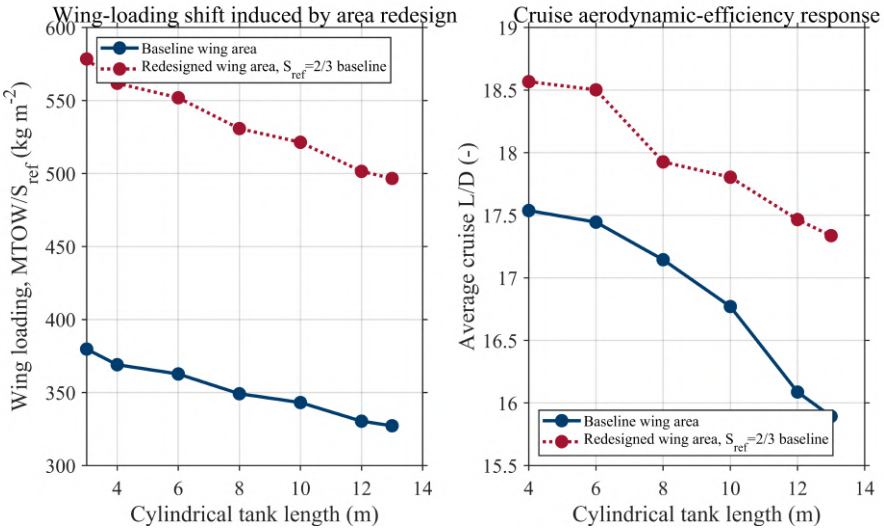


Figure 12 – Wing-loading and average cruise-efficiency response induced by the wing-area reduction.

Figure 13 reports the same comparison as paired differences between the reduced-wing-area and reference families. This representation is useful because the two cases in each pair share the same fuselage and tank length. The positive range difference and the positive average cruise-efficiency difference over the plotted family indicate that the area redesign changes the mission outcome through the aerodynamic design consistency, while the maximum take-off mass difference remains comparatively small and follows from the altered lifting-surface mass and mission sizing. The figure is not a proof that a two-thirds area is the best choice. It is evidence that the workflow can expose a design degree of freedom that is hidden when the airframe is treated as fixed.

The same conclusion is visible in the passenger capacity–range plane, Figure 14. Because the paired cases preserve the same fuselage and tank arrangement, the passenger capacity coordinates remain aligned by construction, whereas the range coordinate changes after aircraft-level design update. The figure therefore separates the volumetric effect of tank intrusion from the aerodynamic and mass-sizing effect of wing-area redesign. For liquid-hydrogen aircraft, where the tanks are likely to be located in the fuselage as in the present cases, the wing box is no longer required to provide the primary volume for the fuel storage. This relaxes a wing-sizing constraint that has been identified as critical in box-wing design studies based on conventional fuel storage [42, 43]. The lifting system can therefore be optimized more directly for aerodynamic, structural and aeroelastic performance, while fuel volume is treated as a fuselage-integration problem.

The 8 m tank-length paired case is further examined through time-resolved mission and tank histories. Figure 15 compares the flight trajectory, lift coefficient, drag coefficient and lift-to-drag ratio for the reference and reduced-wing-area configurations. Both aircraft follow the same nominal mission profile, including climb, cruise, descent and reserve phases, but their aerodynamic operating points differ. The reduced-wing-area variant operates at higher lift coefficients during comparable portions of the mission, as expected from the higher wing loading, and the lift-to-drag history remains above that of the reference case over most of the cruise interval. The result is consistent with the average cruise-efficiency comparison in Figure 12.

The propulsion and hydrogen-use histories in Figure 16 show how the aerodynamic difference propagates to required thrust, hydrogen fuel flow, cumulative venting, burned hydrogen and liquid hydrogen mass. The two cases display similar qualitative mission structure, but the time histories are not identi-

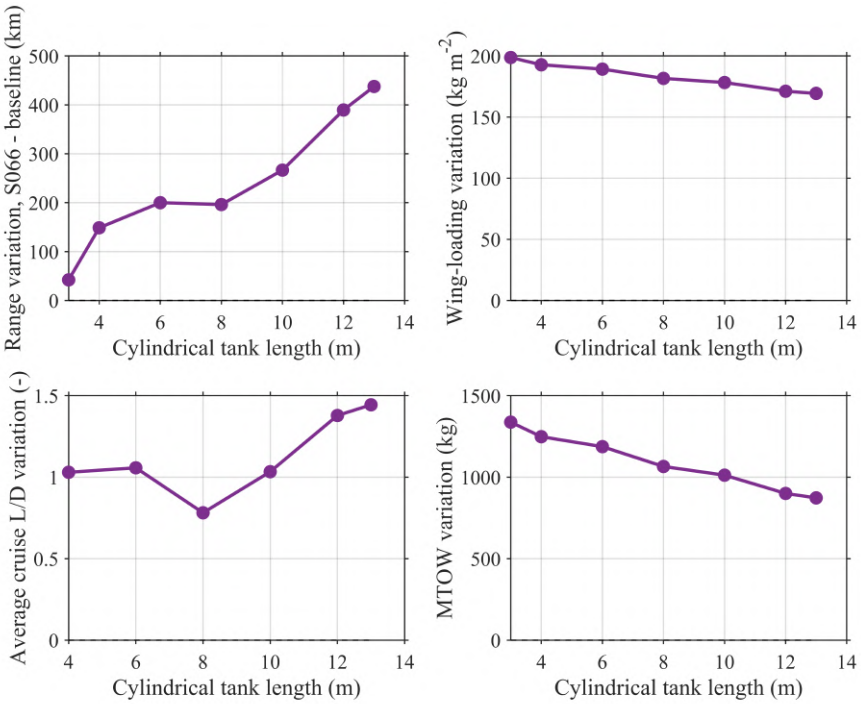


Figure 13 – Paired differences between the reduced-wing-area and reference medium-range families as functions of cylindrical tank length. The graphs show the change in range, wing loading, average cruise lift-to-drag ratio and maximum take-off mass.

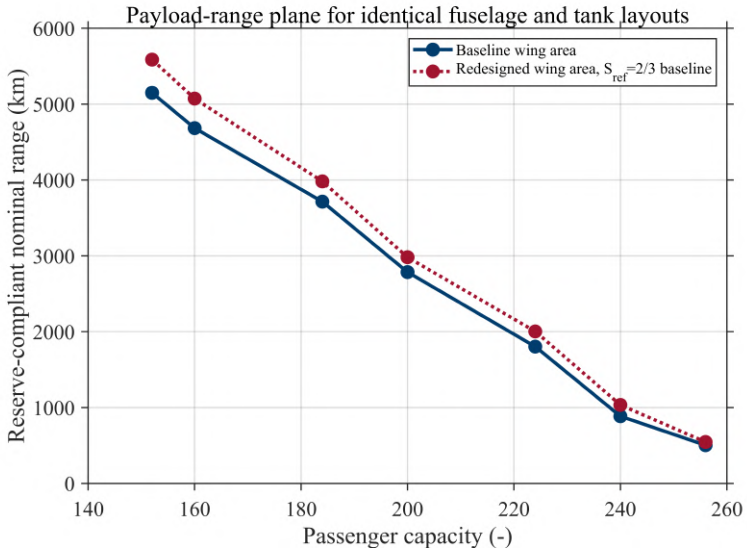


Figure 14 – Payload-range projection for the reference and reduced-wing-area medium-range families.

cal because the different aerodynamic operating point changes the required thrust and fuel flow. The cumulative vented mass remains small on the plotted scale for the 8 m tank-length paired comparison, whereas the burned-hydrogen and liquid-inventory histories reflect the different mission sizing. This figure illustrates why the workflow records both hydrogen burned and hydrogen vented. Only burned hydrogen produces useful propulsive work, while vented hydrogen still reduces aircraft mass and remaining inventory.

Finally, Figure 17 compares tank pressure, thermal load and aircraft mass consumption for the same 8 m tank-length paired case. The pressure histories approach the relief envelope in both configurations, while the heat-load histories remain governed primarily by the mission environment and tank thermal model. The aircraft-mass histories differ because the aircraft-level design consistency and hydrogen consumption differ. The comparison confirms that the redesign is not only an aerodynamic

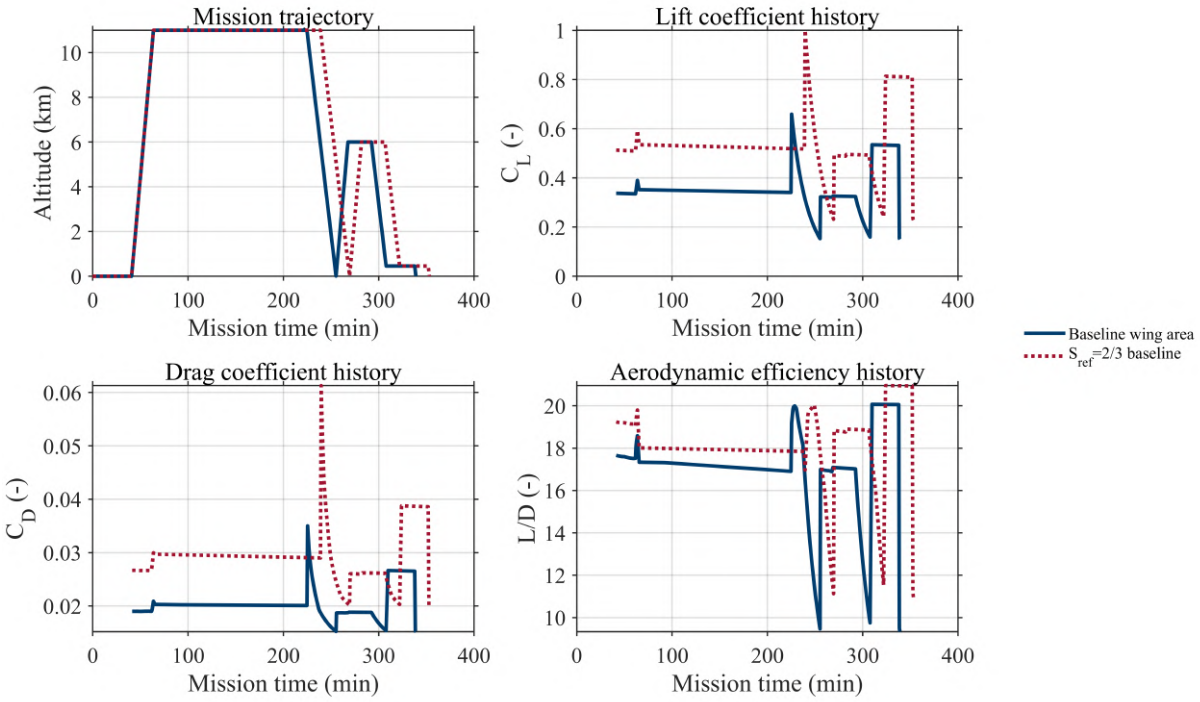


Figure 15 – Time-resolved flight and aerodynamic histories for the reference and reduced-wing-area configurations for the 8 m tank-length case. The graphs compare trajectory, lift coefficient, drag coefficient and lift-to-drag ratio throughout the mission.

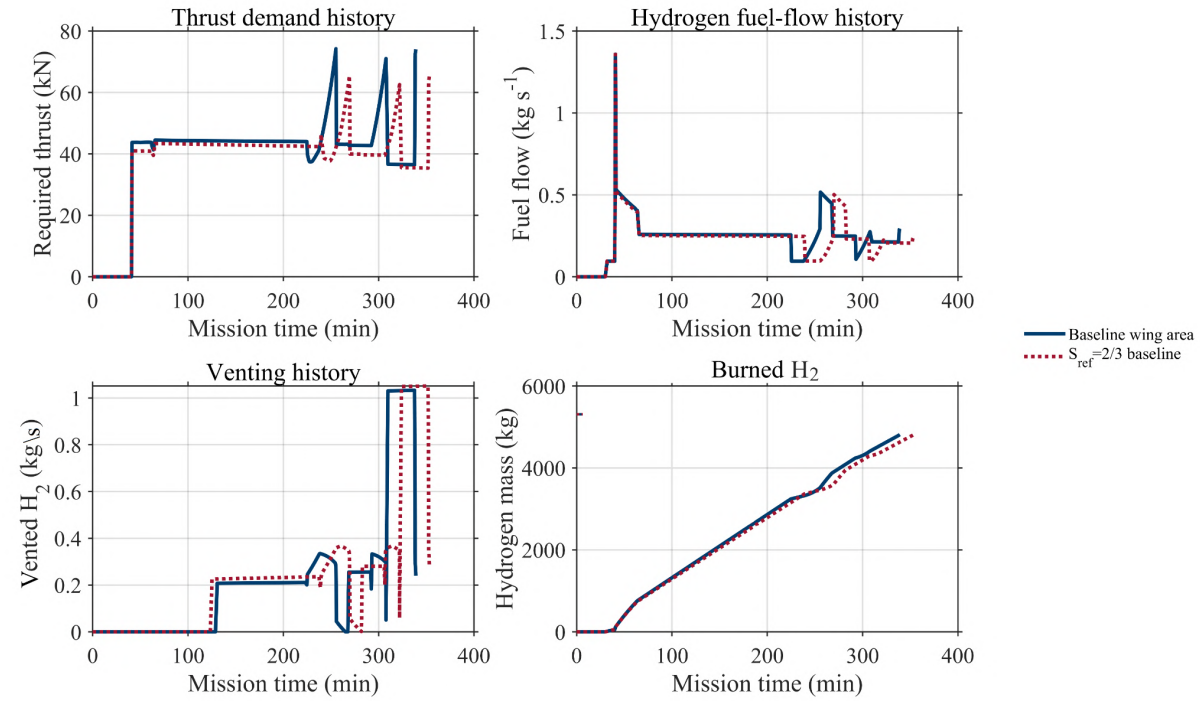


Figure 16 – Propulsion and hydrogen-use histories for the reference and reduced-wing-area configurations for the 8 m tank-length case. The graphs compare required thrust, hydrogen fuel flow, cumulative vented hydrogen and burned hydrogen.

post-processing exercise: it is propagated through the coupled mission and tank simulation.

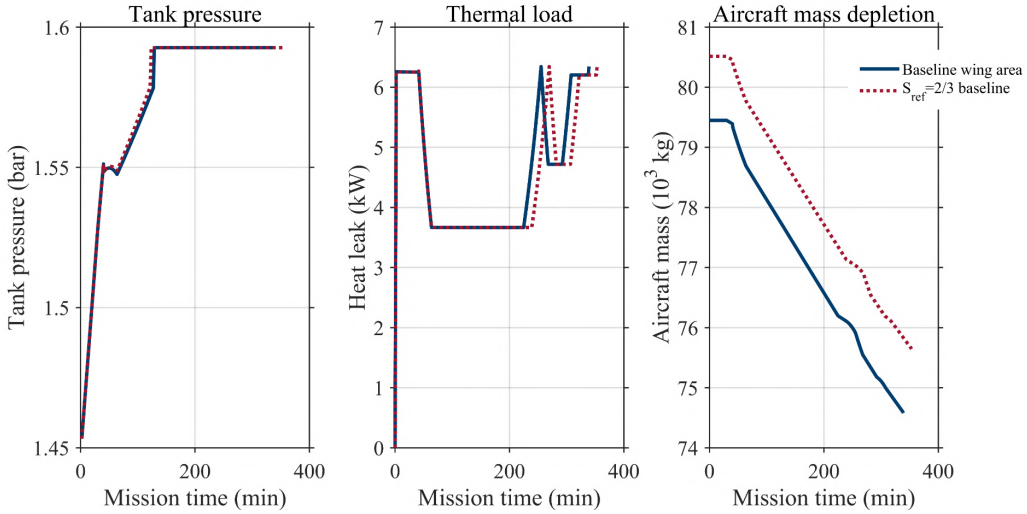


Figure 17 – Thermal and mass-consumption overlay for the reference and reduced-wing-area configurations for the 8 m tank-length case. The graphs compare tank pressure, heat leak and aircraft mass over the coupled mission simulation.

3.3 Tank structural sizing, gravimetric efficiency and cryogenic storage implications

The storage subsystem is not represented within the workflow through a prescribed tank mass fraction. Instead, it is sized on the basis of tank geometry, pressure-vessel design assumptions, insulation modelling, and the structural analyses described in the methodology. Figure 18 summarizes two central outputs of this tank-sizing layer. The dry tank mass increases with cylindrical length, and hence internal volume and initial liquid-hydrogen mass, while the tank gravimetric efficiency decreases with increasing cylindrical tank length over the plotted reference family. Here, tank gravimetric efficiency is defined as the ratio between the initial liquid-hydrogen mass and the sum of initial liquid-hydrogen mass and dry tank mass, $m_{\mathrm{LH2},0}/(m_{\mathrm{LH2},0}+m_{\mathrm{tank,dry}})$. This trend reflects the fact that increasing tank capacity also increases the amount of structural and insulation material that must be carried. The exact values depend on the adopted pressure-vessel model and on the full-section tank geometry, but the methodological point is independent of the specific numbers: the storage penalty is computed and propagated, not prescribed as a fixed external factor.

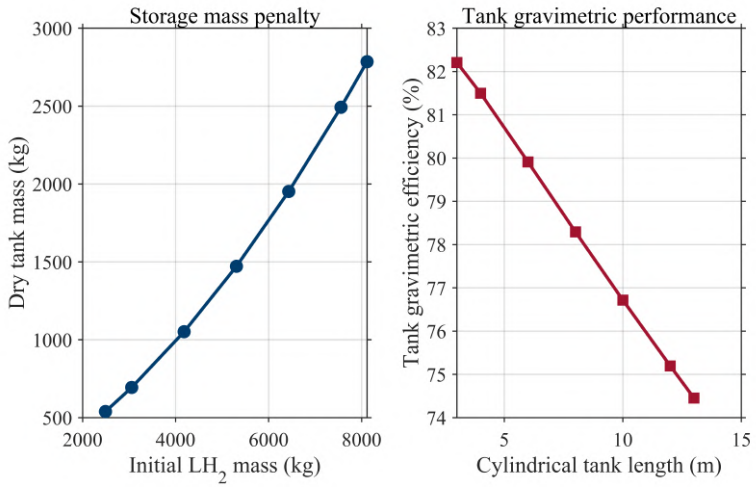


Figure 18 – Tank dry-mass penalty and tank gravimetric efficiency for the reference medium-range family. The graphs report the storage mass response and the resulting tank gravimetric efficiency.

The cryogenic storage implications also depend on thermal-protection choices. Figure 19 compares total vented hydrogen and nominal range for two tank lengths under different insulation thicknesses. For the plotted cases, increasing the insulation thickness reduces vented hydrogen, as expected from

the lower heat leak. At the aircraft level, however, the dominant effect visible in the range comparison is the change in the internal tank volume available for liquid hydrogen: a thicker insulation layer reduces the usable cryogenic volume inside the same fuselage envelope, and this directly lowers the hydrogen mass that can be embarked and, consequently, the nominal range. This is a useful result for conceptual design: insulation cannot be evaluated only by looking at boil-off reduction, and it cannot be selected only by minimizing tank mass. The relevant quantity is the aircraft-level response after the thermal, volumetric and mass consequences have been propagated through the mission.

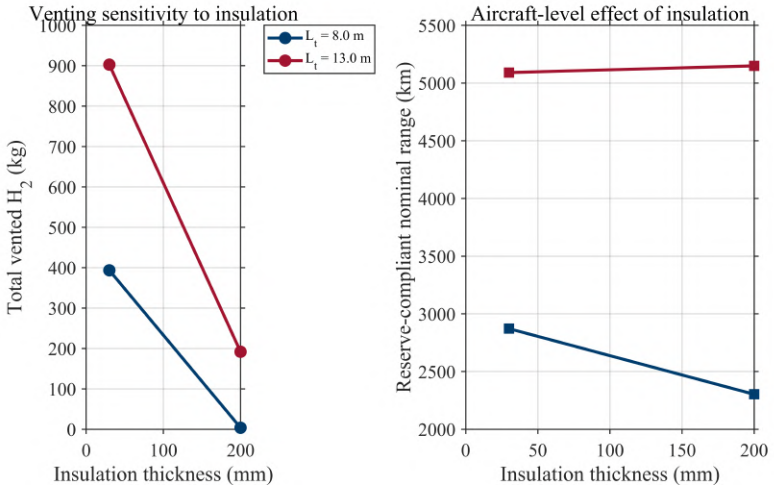


Figure 19 – Sensitivity of vented hydrogen and nominal range to insulation thickness for selected tank lengths.

The pressure-relief setting introduces another operating variable. Figure 20 shows that increasing the venting-pressure factor raises the maximum tank pressure envelope and reduces the total vented hydrogen for the selected case. This behaviour is physically consistent with a larger admissible pressure rise before relief. However, the result should not be interpreted as a recommendation to use the highest pressure setting. Higher pressure affects tank sizing, certification requirements, safety margins and operating procedures; the latter are not fully resolved at conceptual level.

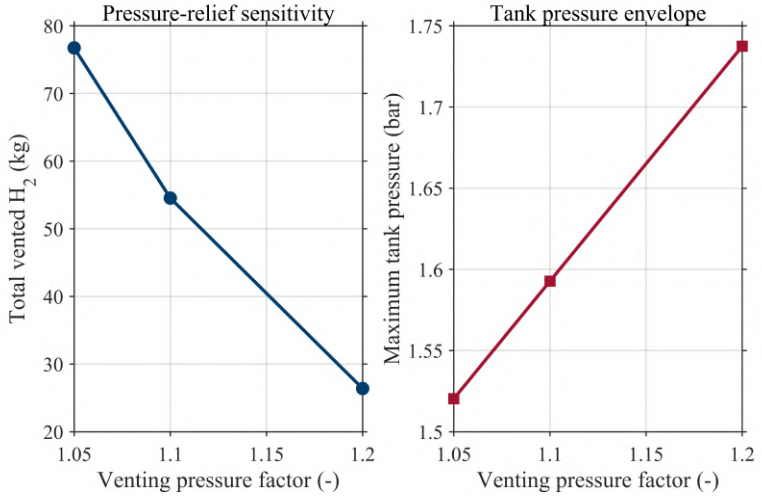


Figure 20 – Sensitivity of total vented hydrogen and maximum tank pressure to the pressure-relief setting. The figure shows the direct coupling between venting setting, tank pressure envelope and hydrogen losses.

The time-resolved storage response associated with insulation choices is shown in Figure 21. The reference baseline case uses an insulation thickness of $t_{\mathrm{ins}} = 80$ mm, while the sensitivity cases replace this value with 30 mm and 200 mm. The pressure histories and venting histories differ among the selected tank-insulation combinations, namely the baseline 8 m reference tank, the 8 m tank with 30 mm insulation and the 8 m tank with 200 mm insulation. The thinner-insulation case reaches

the relief condition earlier and vents more hydrogen, whereas the thicker-insulation case delays or reduces venting. The baseline case lies between these behaviours. This comparison reinforces the interpretation that cryogenic storage is part of the usable-fuel calculation. The initial liquid-hydrogen mass is not sufficient to characterize the aircraft unless heat leak, pressure rise and venting are also tracked during the mission.

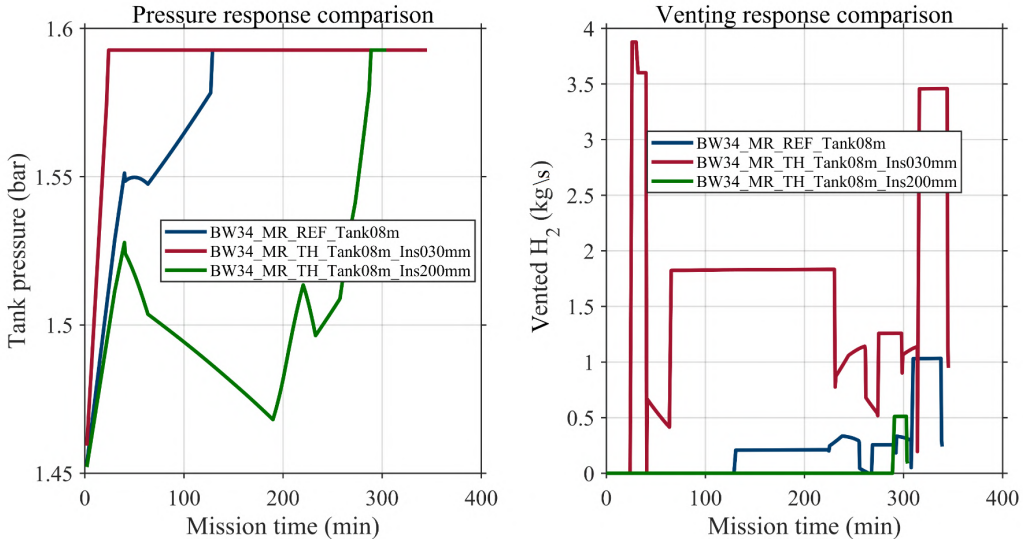


Figure 21 – Selected tank pressure and venting histories for different insulation choices.

3.4 Applicability to different aircraft and airport classes

A conceptual workflow intended for liquid-hydrogen aircraft should not be valid only for a single demonstration aircraft. To assess scalability, the same modelling framework is applied to regional, short-range, medium-range, and long-range box-wing aircraft featuring different tank fractions. In the present results, the tank fraction is defined as L_{tank}/L_f, expressed as a percentage, where L_{tank} is the cylindrical tank length used in the sizing run and L_f is the total fuselage length of the corresponding aircraft. Figure 22 shows an illustrative regional-class layout used in the campaign. Its shorter fuselage and smaller tank envelope make the storage constraint visually different from the medium-range reference case. This example is useful because it makes clear that the same input structure can represent substantially different aircraft scales without changing the global workflow.

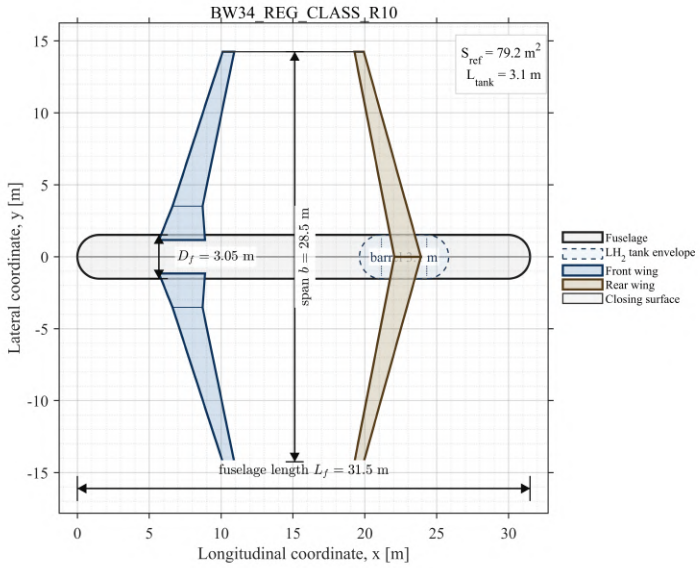


Figure 22 – Illustrative regional-class box-wing layout with a short cylindrical liquid-hydrogen tank.

Figure 23 summarizes the corresponding passenger capacity–range and tank-fraction trends across

aircraft classes. The nominal range capability varies strongly with tank fraction and aircraft scale. Low tank fractions lead to limited range or fuel-limited feasibility boundaries, whereas larger tank fractions increase the nominal range. The slope of each curve changes according to the aircraft class, which is expected because fuselage size, passenger capacity, tank volume, operating empty mass and mission fuel requirement scale differently. The figure is therefore not intended to provide an absolute ranking of the aircraft classes. Rather, its purpose is to demonstrate that the workflow can apply a consistent sizing methodology across different aircraft sizes while revealing nonlinear relationships between storage characteristics and performance.

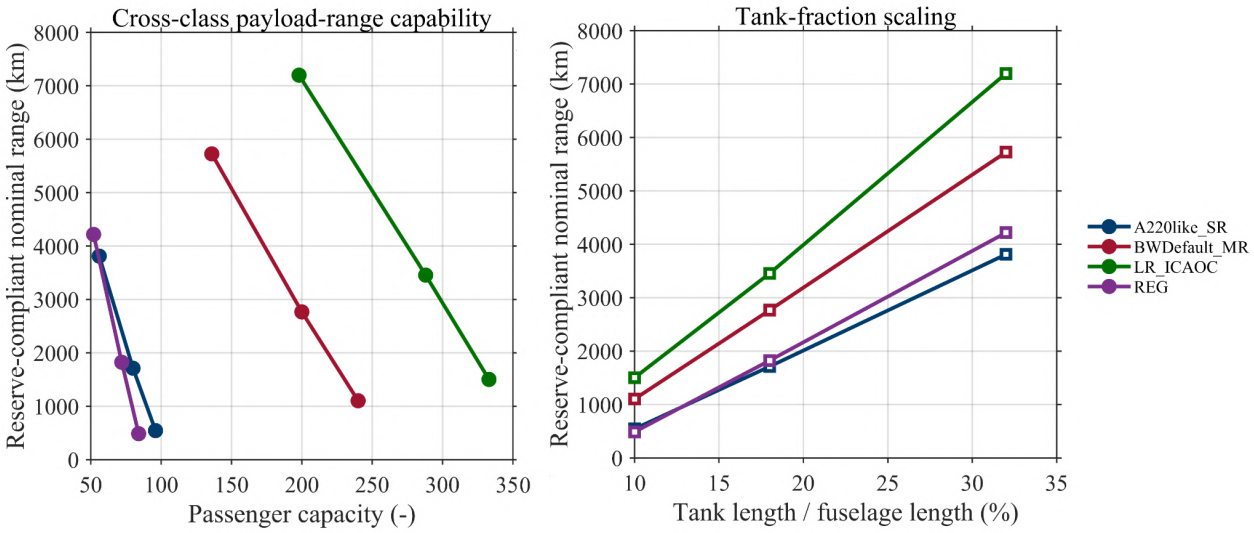


Figure 23 – Cross-class passenger capacity–range capability and tank-fraction scaling for regional-class, short-range, medium-range and long-range box-wing cases.

The aircraft-level metrics in Figure 24 provide the corresponding mass and initial liquid-hydrogen context. Larger aircraft classes require larger mass levels and can accommodate larger liquid-hydrogen masses as the tank fraction increases. At the same time, the relationship between tank fraction, aircraft mass and range is not reducible to a simple proportionality. The same fractional tank length produces different aircraft-level consequences depending on fuselage length and diameter, passenger capacity and mass breakdown.

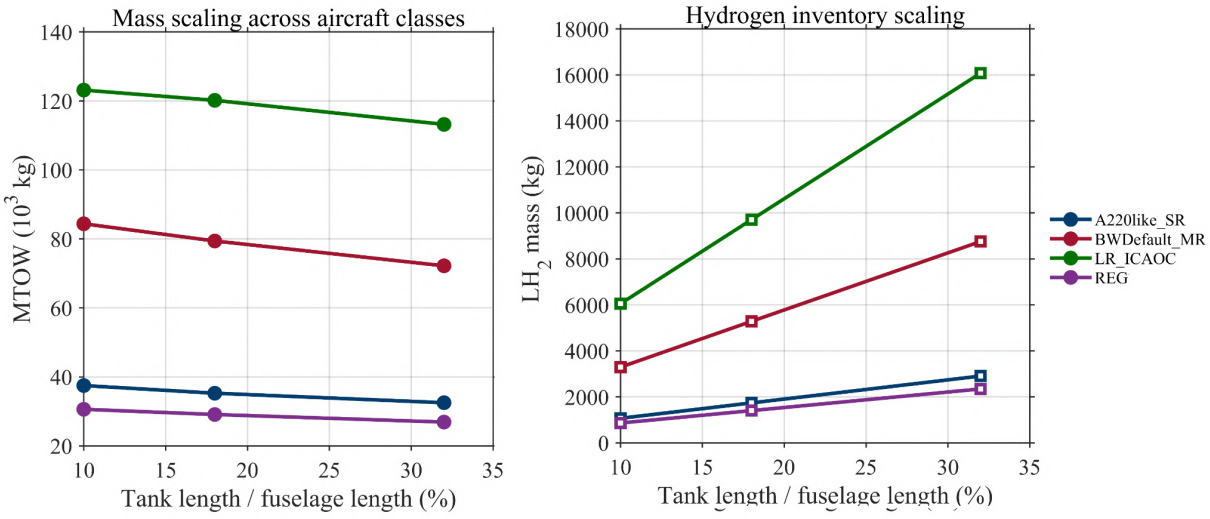


Figure 24 – Mass and initial liquid-hydrogen scaling across the aircraft-class cases.

A second scalability check is performed within an ICAO Code C airport-class constraint. In ICAO

aerodrome reference-code terminology, Code C corresponds to aircraft with wingspan from 24 m up to 36 m [44]; the present example therefore adopts the 36 m class as the limiting span target. Figure 25 shows an ICAO Code C medium-capacity box-wing layout reconstructed from A320-class top-level aircraft requirements and used as one of the comparison cases. In the present paper this comparison is not a tube-and-wing versus box-wing assessment. It is an aircraft-level comparison among conceptual box-wing layouts that remain compatible with the same ICAO Code C airport-class logic.

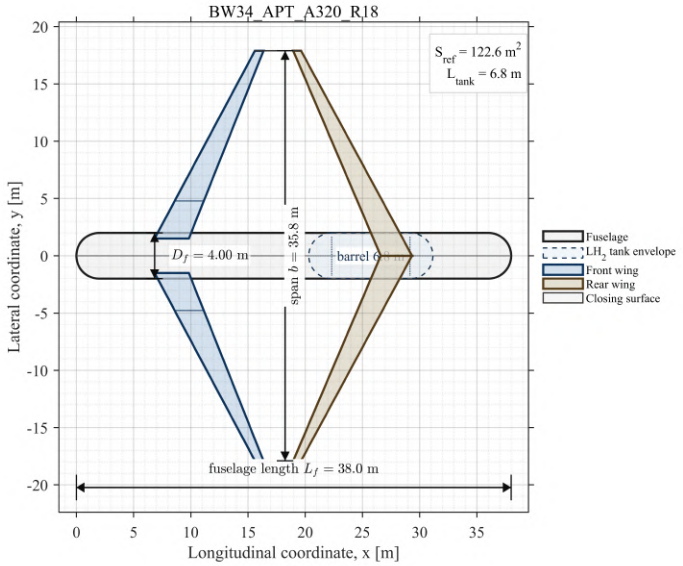


Figure 25 – Illustrative ICAO Code C box-wing layout reconstructed from A320-class top-level aircraft requirements.

Figure 26 compares the nominal passenger capacity–range response of the ICAO Code C box-wing cases. The curves occupy different regions of the passenger capacity–range plane because they are derived from distinct fuselage configurations and capacity assumptions. In the present dataset, this comparison is represented by three fuselage classes: an A220-like narrow-body case, an A320-like narrow-body case and a high-capacity box-wing case. The A220-like case uses a 34.0 m fuselage length, a 3.25 m equivalent fuselage diameter or width, a 2–2 cabin layout, four seats abreast and a 0.78 m seat pitch. The A320-like geometry used for Figure 25 uses a 38.0 m fuselage length, a 4.00 m equivalent fuselage diameter or width, a 3–3 cabin layout, six seats abreast and the same 0.78 m seat pitch. The high-capacity ICAO Code C case uses a 44.2 m fuselage length, a 4.78 m equivalent fuselage diameter or width, a 2–4–2 cabin layout, eight seats abreast and a 0.78 m seat pitch. The passenger capacity coordinates in Figure 26 then reflect the cabin length removed by the selected full-section tank fractions. The high-capacity configuration is particularly informative: for the same span class, it retains the ability to carry a larger, double-aisle-like fuselage while preserving competitive range levels, highlighting one of the architectural opportunities offered by having two different lifting surfaces. Increasing the tank fraction extends the range for each family, but the passenger capacity level and mass state determine the aircraft-level trade. This type of plot is useful for architectural screening because it places storage capability, passenger capacity and nominal range in the same representation.

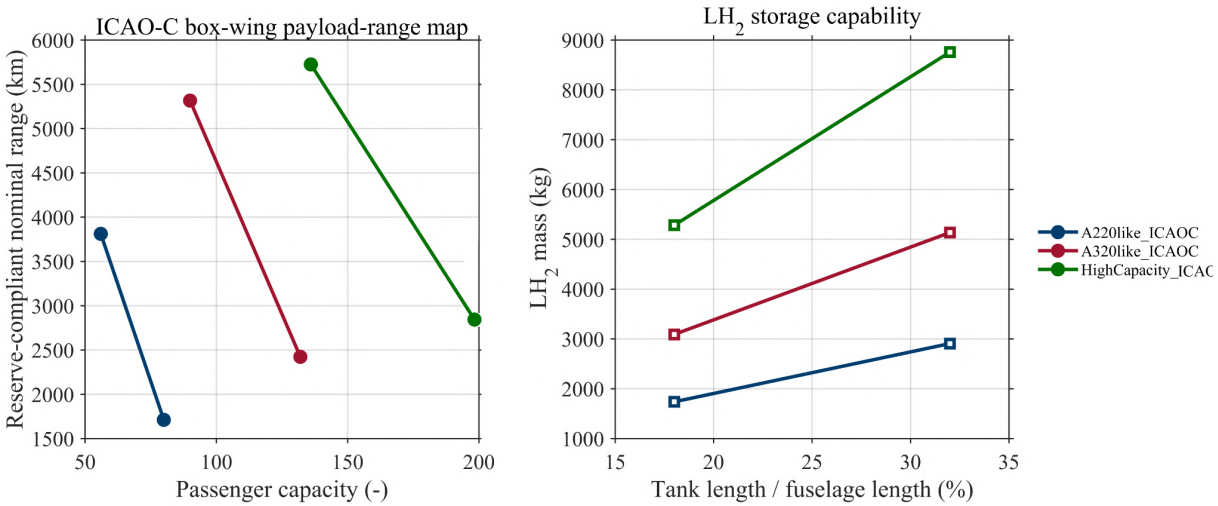


Figure 26 – ICAO Code C box-wing passenger capacity–range comparison. The cases represent different conceptual box-wing layouts within the same span-class logic and with different tank-fraction choices.

3.5 Parametric capability and optimizer or surrogate-readiness

The final set of results employs a design-of-experiments (DOE) dataset to demonstrate the capability of the workflow to generate structured data for subsequent sensitivity analyses, surrogate-model development, and optimization studies. The dataset is not intended to represent a comprehensive optimization campaign, and no final surrogate model is claimed. It is a preliminary parametric sample in which selected independent inputs are perturbed to exercise the coupled workflow. The varied quantities are fuselage length, fuselage diameter, reference area, front/rear area split, installed thrust-to-weight ratio, cruise Mach number, tank fraction, insulation and selected combined variations. The values are prescribed as controlled design points around the reference cases rather than being generated through an optimization loop. Their purpose is to produce converged aircraft configurations from which post-processing, sensitivity studies, and reduced-order modelling procedures can be illustrated.

Figure 27 is introduced as a purely illustrative result. A much larger simulation campaign with a more systematic sampling of the design variables would be required to construct statistically robust DOE maps and reliable surrogate models. The purpose here is narrower: to show the type of coupled aircraft-mission-tank information that the method can produce. The first scatter representation relates nominal range to passenger capacity and uses colour to represent the vented fraction of the initial hydrogen mass. The second relates range to tank length normalized by fuselage length and uses colour to represent tank gravimetric efficiency. The spread of the data points confirms that the workflow generates coupled aircraft, tank, and thermal-performance metrics for each design point. Cases with similar passenger capacity may differ in range because tank fraction, aerodynamic sizing, mass consistency and thermal losses differ. Conversely, cases with similar tank fraction may not have the same range because the aircraft-level state is different. This reinforces the need to map the coupled aircraft-mission-tank design space adequately before extracting reliable reduced-order design information.

Figure 28 provides a preliminary and illustrative reduced-order screening. To make the meaning of the plotted coefficients explicit, the DOE response is approximated by an ordinary least-squares linear model built on standardized input variables and on the standardized converger-computed nominal range,

$$\widehat{\widetilde{R}}_{\mathrm{nom}} = \beta_0 + \sum_{i=1}^{N_v} \beta_i \widetilde{x}_i, \qquad \widetilde{x}_i = \frac{x_i - \mu_{x_i}}{\sigma_{x_i}}, \qquad \widetilde{R}_{\mathrm{nom}} = \frac{R_{\mathrm{nom}} - \mu_R}{\sigma_R}, \tag{52}$$

where R_{nom} is the nominal range, x_i are the sampled DOE input variables, N_v is the number of varied inputs, and μ and σ denote the corresponding sample mean and standard deviation. The coefficients β_i are therefore dimensionless standardized coefficients: their sign indicates whether increasing the

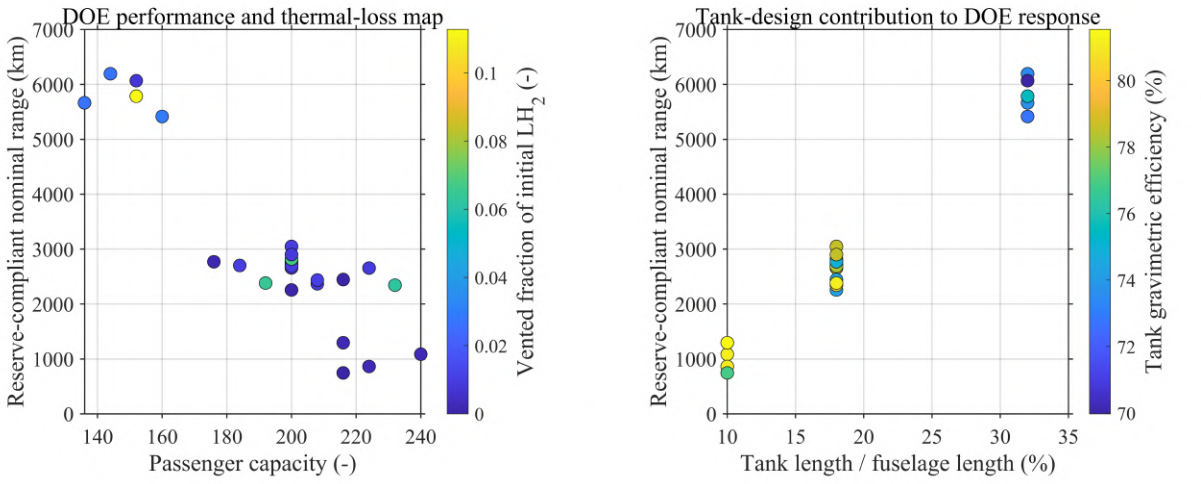


Figure 27 – DOE-based payload-range and tank-response maps. The points combine aircraft-level outputs, storage efficiency and thermodynamic-loss indicators, illustrating the potential of structured datasets produced by the workflow.

corresponding normalized input tends to increase or decrease the nominal range within the sampled dataset, while their magnitude provides a first-order indication of relative influence. The dimensional range prediction shown in the parity plot is obtained by back-transforming the standardized response, $\widehat{R}_{\mathrm{nom}} = \mu_R + \sigma_R \widehat{\widetilde{R}}_{\mathrm{nom}}$. The standardized coefficients therefore indicate trends inside this limited sample, not universal physical sensitivities, and the parity plot checks only the internal consistency of this simple linear approximation. The dominant role of tank fraction in this specific dataset is consistent with the physical importance of liquid-hydrogen volume, but the result remains dataset-dependent. A more complete surrogate would require a larger and more systematic sampling, uncertainty treatment and validation against higher-fidelity disciplinary models, for example following surrogate-modelling strategies already proposed for box-wing structural sizing [41]. The present result should therefore be interpreted only as an example of the data-processing path from converger outputs to reduced-order models, rather than as a validated design surrogate.

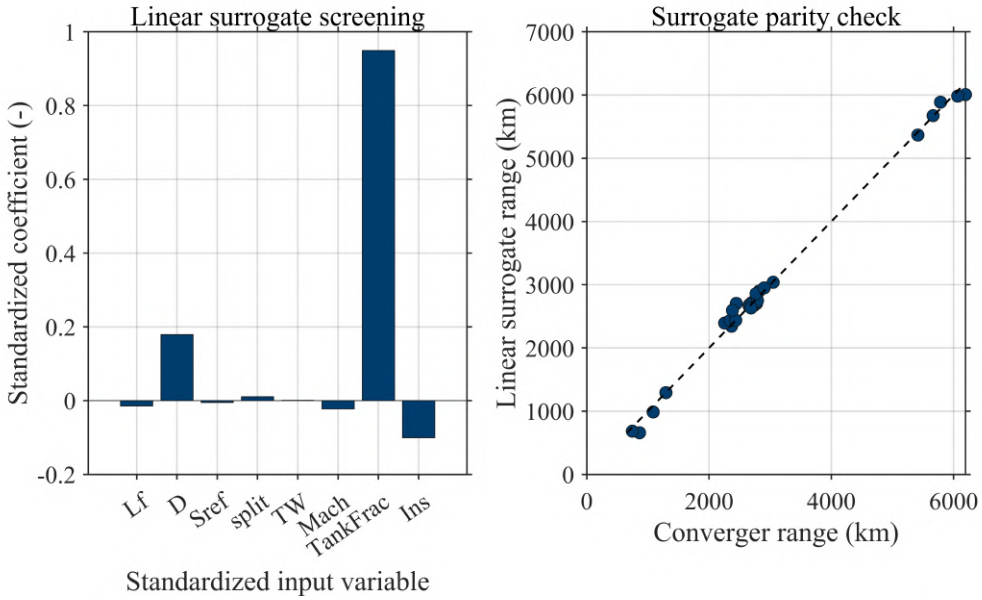


Figure 28 – Preliminary illustrative standardized sensitivity screening and linear-surrogate parity check for the DOE dataset. The coefficients refer to the standardized linear model of Eq. (52).

Beyond surrogate construction, the same workflow can also support direct optimization approaches. Since the input structure is fully parametric, the designer or optimizer can modify fuselage dimen-

sions, lifting-surface variables, tank fraction, insulation settings, cruise conditions and propulsion-sizing assumptions without altering the computational chain. Each candidate design is then evaluated through the same sequence of geometry generation, aerodynamic-performance assessment, mass estimation, tank sizing, coupled mission simulation, thermodynamic update and maximum take-off mass consistency. This makes the tool suitable for gradient-free optimizers, sequential DOE refinement, constrained parametric searches or future multidisciplinary design-optimization frameworks. The important point is that infeasible points and feasible points are generated by the same physics-based accounting logic, so the optimizer can learn not only where the best ranges occur, but also where cabin volume, storage capacity, thermal losses or reserve requirements prevent a consistent liquid-hydrogen aircraft solution.

4. Conclusions and further developments

This paper has presented an integrated conceptual design workflow for liquid-hydrogen-powered box-wing aircraft. The main contribution is methodological: liquid-hydrogen storage is not treated as an external installation added after the airframe has been defined, but as a design driver propagated through geometry, cabin accommodation, tank sizing, mass estimation, mission simulation, tank thermodynamics, reserve assessment and maximum take-off mass consistency. This formulation is particularly relevant for aircraft in which cryogenic tanks are installed in the fuselage, because tank volume directly competes with passenger and cargo volume and indirectly changes payload mass, fuel capacity, take-off mass, aerodynamic operating point and achievable range.

The numerical demonstrations show that the workflow can generate a consistent aircraft state while tracking the separate roles of operating empty weight, payload, dry tank mass, initial liquid-hydrogen mass, burned hydrogen, boil-off, venting and final reserve margin. The reference-family results confirm that increasing tank length is not a simple fuel-capacity change: it simultaneously modifies cabin accommodation, tank structural mass, hydrogen mass, venting and mission range. The reduced-wing-area variation illustrates the importance of redesign-aware analysis. Once the liquid-hydrogen installation changes the mass state of an inherited aircraft, retaining the original lifting-surface area may be suboptimal; regenerating the aerodynamic assessment and resizing the lifting system can reveal performance changes that a retrofit-only study would not expose.

The tank and thermal analyses further show that useful hydrogen availability is governed by more than loaded liquid mass. Heat leak, pressure rise, phase change and venting must be tracked in time if the nominal mission, diversion, holding and final liquid margin are to be assessed consistently. The cross-class, ICAO Code C and DOE examples demonstrate that the same computational backbone can be applied to different aircraft scales and can generate structured datasets for sensitivity analysis, surrogate modelling and direct optimization.

The present framework remains a conceptual design tool. Its aerodynamic database does not replace viscous CFD or detailed transonic and high-lift analyses; the mass models are semi-empirical; the box-wing structural load paths are not yet sized with a dedicated joined-wing structural model; and static stability, trim and control authority are not included in the convergence loop. The tank model also omits detailed support structures, crashworthiness, certification-driven separation rules, thermal stresses, sloshing, active pressure control and spatially resolved multiphase phenomena. Future developments will therefore focus on integrating preliminary stability and trim constraints, replacing selected mass correlations with structural surrogates or FEM-derived metamodels, extending the tank-integration rules to partial-section and distributed layouts, and enriching the propulsion and cryogenic thermal models. These extensions will allow the workflow to move from robust methodological exploration toward higher-fidelity multidisciplinary design optimization of hydrogen-powered box-wing aircraft.

5. Contact Author Email Address

The corresponding author is Karim Abu Salem, mail to: karim.abusalem@unitn.it

6. Copyright Statement

The authors confirm that they, and/or their company or organization, hold copyright on all of the original material included in this paper. The authors also confirm that they have obtained permission,

from the copyright holder of any third party material included in this paper, to publish it as part of their paper. The authors confirm that they give permission, or have obtained permission from the copyright holder of this paper, for the publication and distribution of this paper as part of the ICAS proceedings or as individual off-prints from the proceedings.

References

[1] Ficca A, Marulo F and Sollo A. An open thinking for a vision on sustainable green aviation. *Progress in Aerospace Sciences*, Vol. 141, paper 100928, 2023. doi:10.1016/j.paerosci.2023.100928.

[2] Afonso F, et al. Strategies towards a more sustainable aviation: A systematic review. *Progress in Aerospace Sciences*, Vol. 137, paper 100878, 2023. doi:10.1016/j.paerosci.2022.100878.

[3] Carrera E, Palaia G and Abu Salem K. The green transition in commercial aviation. *Rendiconti Lincei. Scienze Fisiche e Naturali*, Vol. 36, pp. 785–829, 2025. doi:10.1007/s12210-025-01345-1.

[4] Adler EJ and Martins JRRA. Hydrogen-powered aircraft: Fundamental concepts, key technologies, and environmental impacts. *Progress in Aerospace Sciences*, Vol. 141, paper 100922, 2023. doi:10.1016/j.paerosci.2023.100922.

[5] Khandelwal B. Hydrogen powered aircraft: The future of air transport. *Progress in Aerospace Sciences*, Vol. 60, pp. 45–59, 2013. doi:10.1016/j.paerosci.2012.12.002.

[6] Baroutaji A, Wilberforce T, Ramadan M and Olabi A G. Comprehensive investigation on hydrogen and fuel cell technology in the aviation and aerospace sectors. *Renewable and Sustainable Energy Reviews*, Vol. 106, pp. 31–40, 2019. doi:10.1016/j.rser.2019.02.022.

[7] Prewitz M, Bardenhagen A and Beck R. Hydrogen as the fuel of the future in aircrafts: Challenges and opportunities. *International Journal of Hydrogen Energy*, Vol. 45, No. 46, pp. 25378–25385, 2020. doi:10.1016/j.ijhydene.2020.06.238.

[8] Tiwari S, Pekris M J and Doherty J J. A review of liquid hydrogen aircraft and propulsion technologies. *International Journal of Hydrogen Energy*, Vol. 57, pp. 1174–1196, 2024. doi:10.1016/j.ijhydene.2023.12.263.

[9] Gopalasingam D, Rakhshani B and Rodriguez C. Hydrogen propulsion technologies for aviation: A review of fuel cell and direct combustion systems towards decarbonising medium-haul aircraft. *Hydrogen*, Vol. 6, No. 4, paper 92, 2025. doi:10.3390/hydrogen6040092.

[10] Verstraete D. Long range transport aircraft using hydrogen fuel. *International Journal of Hydrogen Energy*, Vol. 38, No. 34, pp. 14824–14831, 2013. doi:10.1016/j.ijhydene.2013.09.021.

[11] Bagarello S, Campagna D and Benedetti I. A survey on hydrogen tanks for sustainable aviation. *Green Energy and Intelligent Transportation*, paper 100224, 2024. doi:10.1016/j.geits.2024.100224.

[12] Bagarello S, Elham A and Benedetti I. Design, optimization, and integration of passively-insulated liquid hydrogen tanks for sustainable aviation. *International Journal of Hydrogen Energy*, Vol. 202, article 153042, 2026. doi:10.1016/j.ijhydene.2025.153042.

[13] Bagarello S, Campagna D and Benedetti I. Computational thermo-mechanical modelling and design-space exploration of cryogenic hydrogen tanks for aviation. *Aerospace Science and Technology*, Vol. 168, Part A, article 110755, 2026. doi:10.1016/j.ast.2025.110755.

[14] Boretti A. Towards hydrogen gas turbine engines aviation: A review of production, infrastructure, storage, aircraft design and combustion technologies. *International Journal of Hydrogen Energy*, Vol. 88, pp. 279–288, 2024. doi:10.1016/j.ijhydene.2024.09.121.

[15] Burschyk T, Cabac Y, Silberhorn D, Boden B and Nagel B. Liquid hydrogen storage design trades for a short-range aircraft concept. *CEAS Aeronautical Journal*, Vol. 14, No. 4, pp. 879–893, 2023. doi:10.1007/s13272-023-00689-4.

[16] Proesmans P and Vos R. Hydrogen medium-range airplane design optimization for minimal global warming impact. *CEAS Aeronautical Journal*, Vol. 15, pp. 781–806, 2024. doi:10.1007/s13272-024-00734-w.

[17] Onorato G, Proesmans P and Hoogreef M F M. Assessment of hydrogen transport aircraft. *CEAS Aeronautical Journal*, Vol. 13, pp. 813–845, 2022. doi:10.1007/s13272-022-00601-6.

[18] Grazioso G, De Marco A, Della Vecchia P, Di Stasio M, Trifari V and Nicolosi F. A simulation-based mission optimization approach for regional transport hybrid-electric aircraft. *Applied Energy*, Vol. 402, article 126869, 2025. doi:10.1016/j.apenergy.2025.126869.

[19] Rischmüller U C J, Lessis A, Egerer P and Hornung M. Conceptual design of a hydrogen-hybrid dual-fuel regional aircraft retrofit. *Aerospace*, Vol. 11, No. 2, paper 123, 2024. doi:10.3390/aerospace11020123.

[20] Rietdijk B and Selier M. Architecture design for a commercially viable hydrogen-electric powered retrofitted regional aircraft. In *Proceedings of the ICAS Conference*, Florence, Italy, 2024.

[21] Palaia G, Abu Salem K, Cipolla V, Zanetti D and Binante V. Conceptual investigation on performance of short-medium range aircraft with liquid hydrogen propulsion and different airframe architectures. *AIAA SCITECH 2023 Forum*, AIAA 2023-0214, 2023. doi:10.2514/6.2023-0214.

[22] Cavallaro R and Demasi L. Challenges, ideas, and innovations of joined-wing configurations: A concept from the past, an opportunity for the future. *Progress in Aerospace Sciences*, Vol. 87, pp. 1–93, 2016. doi:10.1016/j.paerosci.2016.07.002.

[23] Bravo-Mosquera P D, Catalano F M and Zingg D W. Unconventional aircraft for civil aviation: A review of concepts and design methodologies. *Progress in Aerospace Sciences*, Vol. 131, paper 100813, 2022. doi:10.1016/j.paerosci.2022.100813.

[24] Jagtap S S, Childs P R and Stettler M E. Conceptual design-optimisation of a subsonic hydrogen-powered long-range blended-wing-body aircraft. *International Journal of Hydrogen Energy*, Vol. 96, pp. 639–651, 2024. doi:10.1016/j.ijhydene.2024.11.331.

[25] Abu Salem K, Palaia G, Frediani A and Carrera E. The box-wing configuration: a critical review of design approaches and applications. *Progress in Aerospace Sciences*, Vol. 157, paper 101108, 2025. doi:10.1016/j.paerosci.2025.101108.

[26] Prandtl L. Induced drag of multiplanes. NACA Technical Note No. 182, 1924. NASA Document ID 19930080964.

[27] Frediani A and Montanari G. Best wing system: an exact solution of the Prandtl's problem. In *Variational Analysis and Aerospace Engineering*, Springer Optimization and Its Applications, Vol. 33, pp. 183–211, Springer, New York, 2009. doi:10.1007/978-0-387-95857-6_11.

[28] Demasi L. Investigation on the conditions of minimum induced drag of closed wing systems and C-wings. *Journal of Aircraft*, Vol. 44, No. 1, pp. 81–99, 2007. doi:10.2514/1.21884.

[29] Frediani A, Cipolla V and Rizzo E. The PrandtlPlane configuration: overview on possible applications to civil aviation. In *Variational Analysis and Aerospace Engineering: Mathematical Challenges for Aerospace Design*, Springer Optimization and Its Applications, Vol. 66, pp. 179–210, Springer, Boston, 2012. doi:10.1007/978-1-4614-2435-2_8.

[30] Abu Salem K, Cipolla V, Palaia G, Binante V and Zanetti D. A physics-based multidisciplinary approach for the preliminary design and performance analysis of a medium range aircraft with box-wing architecture. *Aerospace*, Vol. 8, No. 10, paper 292, 2021. doi:10.3390/aerospace8100292.

[31] Cipolla V, Zanetti D, Abu Salem K, Binante V and Palaia G. A parametric approach for conceptual integration and performance studies of liquid hydrogen short-medium range aircraft. *Applied Sciences*, Vol. 12, No. 14, paper 6857, 2022. doi:10.3390/app12146857.

[32] Risse K, Schäfer K, Schültke F and Stumpf E. Central reference aircraft data system (CeRAS) for research community. *CEAS Aeronautical Journal*, Vol. 7, pp. 121–133, 2016. doi:10.1007/s13272-015-0177-9.

[33] Palaia G, Abu Salem K and Carrera E. Preliminary performance analysis of medium-range liquid hydrogen-powered box-wing aircraft. *Aerospace*, Vol. 11, No. 5, paper 379, 2024. doi:10.3390/aerospace11050379.

[34] Palaia G, Abu Salem K and Quarta A A. Comparative analysis of hybrid-electric regional aircraft with tube-and-wing and box-wing airframes: a performance study. *Applied Sciences*, Vol. 13, No. 13, paper 7894, 2023. doi:10.3390/app13137894.

[35] Raymer D P. *Aircraft Design: A Conceptual Approach*. 6th ed., AIAA Education Series, American Institute of Aeronautics and Astronautics, Reston, VA, 2018. doi:10.2514/4.104909.

[36] Wells D P, Horvath B L and McCullers L A. *The Flight Optimization System Weights Estimation Method*. NASA/TM-2017-219627/Vol. 1, NASA Langley Research Center, 2017.

[37] ASME. *ASME Boiler and Pressure Vessel Code, Section VIII, Division 1: Rules for Construction of Pressure Vessels*. American Society of Mechanical Engineers, 2023.

[38] International Civil Aviation Organization. *Environmental Protection, Volume II: Aircraft Engine Emissions*. Annex 16 to the Convention on International Civil Aviation, ICAO, Montreal.

[39] Abu Salem K, Palaia G, Quarta A A and Chiarelli M R. Preliminary analysis of the stability and controllability of a box-wing aircraft configuration. *Aerospace*, Vol. 10, No. 10, paper 874, 2023. doi:10.3390/aerospace10100874.

[40] Cipolla V, Binante V, Abu Salem K, Palaia G and Zanetti D. A DoE-based approach for the implementation of structural surrogate models in the early stage design of box-wing aircraft. *Aerospace Science and Technology*, Vol. 117, paper 106968, 2021. doi:10.1016/j.ast.2021.106968.

[41] Palaia G, Abu Salem K, Binante V and Carrera E. Metamodeling approach for wing structural sizing of box-wing aircraft. *Journal of Aircraft*, 2025. doi:10.2514/1.C038131.

[42] Schiktanz D and Scholz D. Box wing fundamentals: An aircraft design perspective. DGLR Deutscher Luft- und Raumfahrtkongress, pp. 601-615, 2011.

[43] Andrews S A and Perez R E. Comparison of box-wing and conventional aircraft mission performance using multidisciplinary analysis and optimization. Aerospace Science and Technology, Vol. 79, pp. 336-351, 2018. doi:10.1016/j.ast.2018.05.060.

[44] International Civil Aviation Organization. Aerodromes, Volume I: Aerodrome Design and Operations. Annex 14 to the Convention on International Civil Aviation, ICAO, Montreal.